cogent
geoscience

*Corresponding author. Robert J. Holm, Frogtech Geoscience, 2 King Street, Deakin West ACT 2600, Australia; Geosciences, College of Science & Engineering, James Cook University, Townsville, Queensland 4811, Australia
E-mail: rholm@frogtech.com.au

SOLID EARTH SCIENCES | RESEARCH ARTICLE

Petrology and crustal inheritance of the Cloudy Bay Volcanics as derived from a fluvial conglomerate, Papuan Peninsula (Papua New Guinea): An example of geological inquiry in the absence of *in situ* outcrop

Robert J. Holm[1,2]* and Benny Poke[3]

Abstract: In regions of enhanced weathering and erosion, such as Papua New Guinea, our ability to examine a complete geological record can become compromised by the absence of *in situ* outcrops. In this study, we provide an example of the insights that can be gained from investigations of secondary deposits. We sampled matrix material and clasts derived from an isolated conglomerate outcrop within a landscape dominated by lowland tropical forest of the southeast Papuan Peninsula, and mapped as belonging to the Cloudy Bay Volcanics. Nine variations of volcanic rock types were identified that range from basalts to trachyandesites. Major and trace element geochemistry characterize the volcanic arc assemblage as shoshonites and provide evidence for differential magma evolution pathways with a subset of samples marked by heavy REE- and Y-depletion, indicative of high-pressure magma fractionation. Zircon U–Pb dating of the individual volcanic clasts indicates activity of the Cloudy Bay Volcanics was largely constrained to the latest Miocene, between ca. 7 and 5 Ma. Of the analyzed zircons, the majority are xenocrystic

ABOUT THE AUTHORS

Robert J. Holm is a senior geoscientist with Frogtech Geoscience and an adjunct lecturer in Geosciences at James Cook University. Robert is an early career geoscientist interested in multidisciplinary and innovative approaches to solve earth science problems, and holds expertise in the research areas of tectonics, igneous petrology, structural geology, geochronology, and metallogeneis. He obtained his PhD from James Cook University, investigating magmatic arcs and porphyry systems of Papua New Guinea to gain new insights into the late Cenozoic tectono-magmatic evolution and subduction histories at the northern Australian plate boundary. Robert continues his research into the South West Pacific and is working toward developing an integrated approach to geosciences in the region and developing collaborations between regional universities, government agencies, together with the minerals, and oil and gas industries to benefit our understanding of the regional geology.

PUBLIC INTEREST STATEMENT

Plate tectonics have shaped the Earth and give rise to natural hazards such as earthquakes and volcanoes. To understand how the Earth changes through time we observe these processes, such as volcanism and magmatism in the geological rock record, and investigate how changes in these processes reflect large-scale changes related to plate tectonics. However, Earth surface processes such as weathering and erosion that shape the landscape will often obscure or remove the rocks that are required to investigate the geological record for a specific region. In this study, we implement an innovative methodology of sampling conglomerates, or river deposits, eroded from ancient volcanic activity in Papua New Guinea. By investigating individual rock clasts within these deposits, we explore ancient volcanic activity and reveal what insights we can gain into the wider formation and evolution of the region up to the present day.

cogent • geoscience

zircons that provide insight into the provenance of the Papuan Peninsula with potentially significant implications for South West Pacific tectonics. Additional Hf-isotope analysis of the primary igneous zircons suggests a relatively unradiogenic crustal component contributed to magma compositions, which cannot be readily explained by current regional tectonic paradigms.

**Subjects: Earth Sciences; Tectonics; Mineralogy & Petrology; Volcanology; Sedimentology & Stratigraphy**

Keywords: Papua New Guinea; volcanic; conglomerate; shoshonite; U–Pb geochronology; zircon provenance; Hf isotope

1. Introduction

In regions of enhanced weathering and erosion our ability to examine the geological record can become compromised by earth surface processes. These processes can include, for example, deep weathering profiles, obstruction beneath cover, or removal via erosion, and are typical of tropical climates and areas of active tectonics and uplift. As a result, these areas are often characterized by gaps in our data-sets and difficulties in reconciling the regional geological history. Investigations into the petrology of first-generation conglomerate clasts, such as presented in this study, can offer many insights into the nature of rocks exposed in their source catchment at the time of deposition (e.g. Lamminen, Andersen, & Nystuen, 2015; Samuel, Be'eri-Shlevin, Azer, Whitehouse, & Moussa, 2011; Schott & Johnson, 2001). The power of this methodology is derived in part from sedimentary processes where clastic detrital material records the bedrock geology that is representative of a larger watershed or geological terrain. For example, parameters such as age, texture, or composition for a group of conglomerate clasts can be useful in identifying not only the source of the detritus and associated sedimentary pathways (e.g. detrital zircon provenance; Gehrels, 2014), but also provide us with detailed insights into the nature of terranes that have been lost to erosion, burial, or tectonic dismemberment (e.g. Graham & Korsch, 1990; Hidaka, Shimizu, & Adachi, 2002; Lamminen et al., 2015; Samuel et al., 2011; Schott & Johnson, 2001; Wandres et al., 2004).

In this study, rather than surface processes obscuring geological information, we use fluvial and colluvial surface processes, and the resulting secondary deposits, to complement existing data-sets and contribute to our understanding of a geological terrane. We report the results of an investigation into an outcrop of conglomerate within an area previously mapped as part of the Cloudy Bay Volcanics of the southeast Papuan Peninsula of Papua New Guinea (Figure 1). The chosen sample location on the southern coast of the Papuan Peninsula provides an example of a terrain where exploring the geological history of the region through traditional ground-based geological mapping techniques is extremely difficult, if not impossible. The terrain is characterized by dense lowland tropical forest with regional swamp forest and mangroves, with moderately high rainfall (750–1,200-mm precipitation in the driest quarter; Shearman, Ash, Mackey, Bryan, & Lokes, 2009; Shearman & Bryan, 2011). Such conditions are characteristic of tropical regions, such as Papua New Guinea, where dense vegetation and thick soil profiles result in a low density of informative outcrops. In this example, the sampled assemblage of clasts and matrix material were examined via zircon U–Pb geochronology, zircon Lu–Hf isotope analysis, and whole-rock major and trace element geochemical investigations. The results from this work demonstrate that in areas where suitable *in situ* outcrops may be absent or compromised by earth surface processes, we can still gain valuable insight into the wider geological history of a region through targeted and innovative sampling methodologies. The investigation presented here is part of a wider examination of the geology of southeast Papua New Guinea, in which, we aim to demonstrate the regional tectonic insights that can be gained from such sampling of secondary deposits.

cogent · geoscience

Figure 1. Topography, bathymetry, and major tectonic boundaries of southeast Papua New Guinea and the Papuan Peninsula region. (A) tectonic elements of the southeast Papua New Guinea region (modified from Holm et al., 2016); NBT, New Britain trench; NGMB, New Guinea Mobile Belt; TT, Trobriand trough. Topography and bathymetry after Amante and Eakins (2009). (B) landscape morphology of the Cloudy Bay area and position of the sample site in the lowland rainforest. (C) Miocene to Quaternary volcanic and intrusive rocks of southeast Papua New Guinea (modified from Australian BMR, Australian Bureau of Mineral Resources, 1972; Smith & Milsom, 1984). Inset shows location of B).
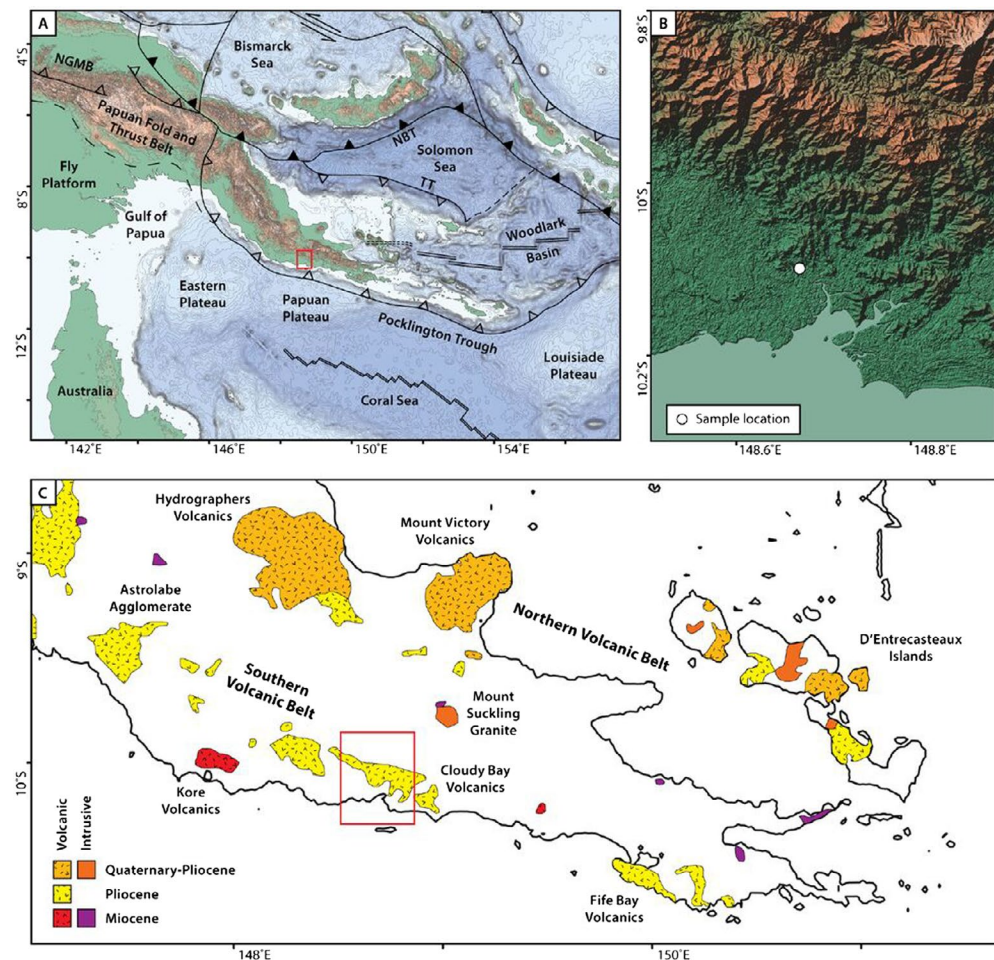
2. Geologic setting and samples

2.1. Geological setting

The Papuan Peninsula forms the eastern extent of the Papua New Guinea mainland, between approximately 146 and 151°E (Figure 1). There are two main components that comprise the geological basement of the Papuan Peninsula. These are a core of moderate to high-grade metamorphic rocks, that form the Owen Stanley Metamorphic Complex that transitions into the Milne Terrane to the east, and the overlying Papuan Ultramafic Belt; an obducted sheet of ultramafic rocks and associated mid-ocean ridge-type basalts (Baldwin, Fitzgerald, & Webb, 2012; Davies, 2012; Davies & Smith, 1971; Smith, 2013a).

The Owen Stanley Metamorphic Complex forms the main spine of the Owen Stanley Ranges and the Papuan Peninsula. Two major rock units form the Owen Stanley Metamorphic Complex. The Kagi Metamorphics are primarily composed of pelitic and psammitic sediments derived from felsic volcanism, with minor intercalated volcanics, that have been folded and metamorphosed to greenschist facies (Davies, 2012; Pieters, 1978). The Emo Metamorphics outcrop northeast of, and overlie the Kagi Metamorphics, forming a 1–2-km-thick carapace, which dips shallowly to the north and northeast. The Emo Metamorphics mainly comprise metabasite derived from low-K tholeiitic basalt, dolerite, and gabbro, together with minor volcaniclastic sediments, and metamorphosed to greenschist and blueschist metamorphic facies (Davies, 2012; Pieters, 1978). The protolith of the Emo Metamorphics is interpreted as a supra-subduction extensional back arc setting (Smith, 2013a; Worthing & Crawford, 1996). The Owen Stanley Metamorphic Complex is interpreted to be of middle

Cretaceous age from U–Pb dating of zircon of likely volcanic origin (Aptian–Albian; 120–107 Ma [Kopi, Findlay, & Williams, 2000]), and from preserved macrofossils (Aptian–Cenomanian [Dow, Smit, & Page, 1974]).

The Milne Terrane occupies the equivalent structural domain to the Owen Stanley Metamorphics in the southeast of the Papuan Peninsula and comprises the Goropu Metabasalt and Kutu Volcanics (Smith, 2013a; Worthing & Crawford, 1996). The Goropu Metabasalt consists of low-grade N-MORB-type metabasalts with minor metamorphosed limestone and calcareous schist. Submarine basaltic volcanoes and interbedded lenses of pelagic limestone with minor terrigenous sediments form the interpreted protolith for the Goropu Metabasalt (Smith, 2013a; Smith & Davies, 1976). The Kutu Volcanics are interpreted as the unmetamorphosed continuation of the Goropu Metabasalt comprising dominantly basaltic lava with minor gabbro and ultramafics, agglomerate, tuffaceous and calcareous sediments, and limestone (Smith, 2013a; Smith & Davies, 1976). The age of the Milne Terrane is constrained by microfossils and is interpreted to have been deposited from the Upper Cretaceous (Maestrictian), and potentially as young as Eocene in the southeast of the terrane (Smith & Davies, 1976).

The Papuan Ultramafic Belt occupies the northeast side of the Papuan Peninsula and is juxtaposed above the Owen Stanley Metamorphic Complex along the Owen Stanley Fault (Baldwin et al., 2012; Davies, 2012). The Papuan Ultramafic Belt is interpreted as an ophiolite complex comprising oceanic crust and lithospheric mantle (Davies & Jaques, 1984; Davies & Smith, 1971), which is interpreted as late Cretaceous in age (Davies, 2012; Davies & Smith, 1971). Obduction of the Papuan Ultramafic Belt, and metamorphism of the Owen Stanley Metamorphic Complex, is interpreted at 58.3 ± 0.4 Ma, derived from the cooling age of amphibole within the high-grade metamorphic contact between the two terranes (Davies, 2012; Lus, McDougall, & Davies, 2004).

The Papuan Peninsula was subsequently intruded by a major episode of subduction-related volcanism, which commenced during the middle Miocene and has continued to the present day (e.g. Jakeš & Smith, 1970; Smith, 1972, 1982, 2013b; Smith & Milsom, 1984). This volcanic province is marked by a transition from early submarine–subaerial activity, to entirely subaerial volcanism during the Pliocene and Quaternary, reflecting the emergence of eastern Papua New Guinea during the latter part of the Cenozoic (Davies, 2012).

The Cloudy Bay Volcanics are located some 140 km east-southeast from Port Moresby and extend a further 90 km east along the Papuan Peninsula (Figure 1). The volcanics cover approximately 770 km^2 and form rolling terrain with very low relief, and extend up to the foothills of the Milne Terrane at an elevation of ca. 250 m. The estimated thickness of the volcanics is 500 m, and they dip at a shallow angle to the south (Pieters, 1978). Mapping of the Cloudy Bay Volcanics suggests it mainly comprises basalt, andesitic pyroclastics and lava, and tuffaceous sandstone (Pieters, 1978; Smith, 1976). The tuff-dominated members form rolling terrain with very low relief and moderately spaced meandering streams, whereas the lava and pyroclastic members form small cones, and are associated with greater relief and dendritic drainage patterns (Pieters, 1978).

2.2. Samples

In this study, we sampled a single isolated conglomerate outcrop (Figure 2; 10.102°S 148.673°E) within a landscape dominated by lowland rainforest and swamp, and mapped as part of the Cloudy Bay Volcanics (Figure 1). The outcrop comprised a clast-supported conglomerate and was sampled for clasts of different rock types, together with samples of the matrix. Clasts within the outcrop were predominantly cobble and boulder-sized up to approximately 50 cm in diameter, typically subrounded to well-rounded, and elongated to spherical in shape (Figure 2). The matrix material was dominantly made up of clays but also contained recognizable, euhedral plagioclase and pyroxene grains, indicating the detritus was immature and not well-traveled. From the isolated nature of the outcrop it is difficult to establish its context within the Cloudy Bay Volcanics, however, it likely represents a secondary deposit derived from fluvial transport of an eroding volcanic landscape.

Figure 2. Conglomerate outcrop from which samples were collected for this study. Outcrop location is shown in inset of Figure 1. Lens cap used for scale in lower center of the photograph is 46 mm diameter.


In the field, an effort was made to collect a representative variety of clast types that reflected the compositional variation within the outcrop, but were also sufficiently large to conduct analytical procedures. In total, nine clasts types were identified and sampled, in addition to the matrix. Given the weathered and degraded appearance of the clasts in the field (see supplementary material for sample photographs), rock descriptions and petrography were carried out on the least altered rock material following processing (Figure 3; Table 1). All the sampled clasts comprise mafic-intermediate volcanic rock types, which range in composition from basalt to trachyandesite. Most samples are porphyritic in texture with a very fine-grained to aphanitic matrix; samples 103265 and 103267 comprise augite phenocrysts up to 5 mm in length, in a very fine-grained matrix; the remaining samples predominantly consist of plagioclase- and augite-phyric lavas where the phenocryst size is <2 mm. Magnetite (<0.5 mm) and biotite (typically <2 mm) phenocrysts are also present in various samples (Table 1); apatite crystals up to 1 mm are present in sample 103265. The matrix of the selected volcanic samples comprises similar mineralogy, made up of variable amounts of plagioclase, augite, magnetite, apatite, and biotite. Sample 102368c is textually distinct within the sample suite being very fine grained to aphanitic in nature, although augite, plagioclase, magnetite, and apatite microphenocrysts can be identified.

3. Methods

Samples of both clasts and matrix material were collected from the conglomerate outcrop shown in Figure 2. Rock clasts were washed to remove any contamination from matrix material and soil, cut into workable sections, and weathering rinds were removed with diamond implanted grinders. The least weathered material from each clast was selected for petrographic thin sections and geochemical analysis. The amount of rock material sampled for geochemical analysis ranged from 110 g up to 240 g (average of 170 g) depending on the size and weathering state of the clast. The remainder of each sample, including weathered sections free from matrix material and soil contamination, was subsequently utilized for mineral separation. Matrix material predominantly comprised clay with lithic pebbles and remnant minerals. The matrix sample was dried over several days at 100°C before

Figure 3. Petrographic mosaic photographs for selected samples used in this study (additional samples are included in the supplementary material). For each sample, the image on the left is observed under plane-polarized light, and the right under cross-polarized light. See Table 1 for sample descriptions.
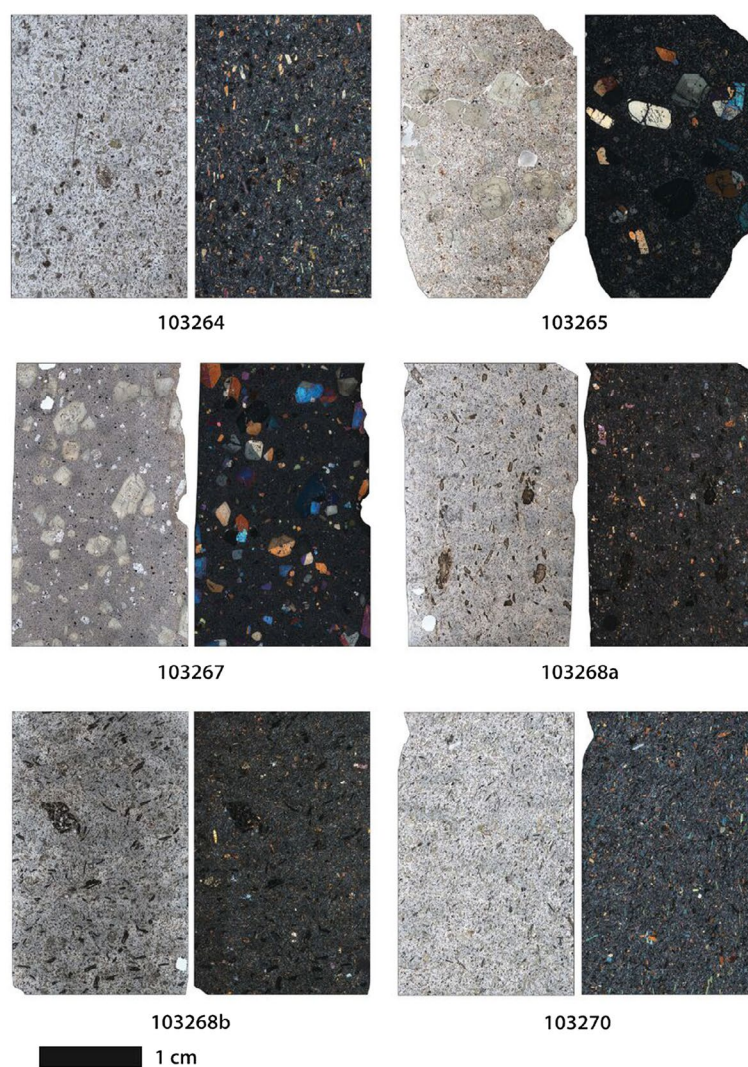
undergoing mineral separation as a bulk sample. The matrix material was not amenable to petrographic thin section preparation.

All geochemical analyses were carried out by the Bureau Veritas Mineral Laboratories in Vancouver, Canada. Whole rock samples were crushed, split, and pulverized to a 200-mesh grain size, and mixed with $LiBO_2/Li_2B_4O_7$ flux. The cooled bead was dissolved in ACS grade nitric acid and analyzed by a combination of ICP-ES and ICP-MS methods. Additional volatile elements (Mo, Cu, Pb, Zn, Ni, As) were analyzed via aqua regia digestion in combination with ICP-ES and ICP-MS instrumentation. In-house standards (SO-19 and DS10) were used to measure analytical uncertainty. The maximum errors for SiO_2, MgO, and K_2O were 1.0, 1.0, and 3.9%, respectively. Maximum relative errors for representative trace elements Nb, Zr, Y, Nd, and Sm are 3.8, 5.3, 8.2, 8.6, and 11.3%, respectively. The relative errors for other trace elements were similar in magnitude based on a comparison between the measured and accepted trace element concentrations. Loss on ignition (LOI) was determined by igniting a 1-g sample split to 1,000°C for one hour, cooled and then measuring the weight loss.

Mineral separation to extract zircon crystals was carried out at James Cook University (JCU) in a standard process. Samples were crushed and milled to 500 μm, and separation was carried out via the use of a Wilfley table (smaller samples were hand washed to remove the clay fraction), and a

Table 1. Sample descriptions				
Sample	**TAS Classification**	**Phenocrysts**	**Matrix**	**Additional Notes**
103264	basaltic trachyandesite	Aug + Mag + Ap + Bt	Pl + Mag + Ap	Mag + Bt + Aug aggregates
103265	basalt	Aug + Ap + Mag	Pl + Ap + Mag + Bt	Hem rims on Ap
103267	trachybasalt	Aug + Mag	Pl + Aug + Mag + Ap	2 Aug phenocryst generations
103268a	basaltic trachyandesite	Aug + Pl + Mag + Bt	Pl + Mag + Ap	Pl + Aug + Bt + Mag + Ap aggregates
				Pl phenocryst breakdown
103268b	trachyandesite	Aug + Pl + Mag	Pl + Aug + Mag + Ap	Pl + Aug + Bt + Mag + Ap aggregates
				Pl phenocryst breakdown
103268c	basalt	no phenocrysts	Aug + Pl + Mag + Ap	Aug xenocryst
103268d	basaltic trachyandesite	Aug + Pl + Mag	Pl + Mag + Ap	Pl + Aug + Bt + Mag + Ap aggregates
				Pl phenocryst breakdown
103269	trachyandesite	Pl + Aug + Mag	Pl + Aug + Mag + Ap	Aug + Mag + Bt + Ap aggregates
				minor Pl phenocryst breakdown
103270	basaltic trachyandesite	Aug + Pl + Mag + Bt	Pl + Mag + Aug + Ap	alignment of phenocrysts and matrix
				Aug + Mag + Bt + Ap aggregates

Notes: Mineral codes: Aug, augite; Mag, magnetite; Ap, apatite; Bt, biotite; Pl, plagioclase; Hem, hematite.

combination of heavy liquid density separation and magnetic separation. Zircon crystals were hand-picked under a binocular microscope and mounted in epoxy, before being polished and carbon-coated. Cathodoluminescence (CL) images of all zircon crystals were obtained to study internal zonation and structures using a Jeol JSM5410LV scanning electron microscope equipped with a Robinson CL detector, housed at the Advanced Analytical Centre (AAC), JCU (Figure. 4; additionally see supplementary material for complete CL images).

All U–Pb dating work was completed at the AAC, JCU. U–Pb dating of zircons was conducted via Coherent GeolasPro 193 nm ArF Excimer laser ablation system connected to a Bruker 820-ICP-MS following the methodology outlined in Holm, Spandler, and Richards (2013, 2015). All zircons were analyzed with a beam spot diameter of 44 μm and selection of analytical sample spots was guided by CL images. Data reduction was carried out using the Glitter software (Van Achterbergh, Ryan, Jackson, & Griffin, 2001). Drift in instrumental measurements was corrected following analysis of drift trends in the raw data using measured values for the GJ1 primary zircon standard (608.5 ± 0.4 Ma; Jackson, Pearson, Griffin, & Belousova, 2004). Secondary zircon standards Temora 2 (416.8 ± 0.3 Ma; Black et al., 2004) and AusZ2 (38.8963 ± 0.0044 Ma; Kennedy, Wotzlaw, Schaltegger, Crowley, & Schmitz, 2014) were used for verification of GJ1 following drift correction (see supplementary material). For quantification of U and Th concentration in zircon samples, analysis of the NIST SRM 612 reference glass was conducted throughout every analytical session at regular intervals, with ^{29}Si used as the internal standard assuming perfect zircon stoichiometry. Background corrected analytical count rates, calculated isotopic ratios and 1σ uncertainties were exported for further processing and data reduction.

Age regression and data presentation for all samples was carried out using Isoplot (Ludwig, 2009). Correction for initial Th/U disequilibrium during zircon crystallization related to the exclusion of ^{230}Th due to isotope fractionation, and resulting in a deficit of measured ^{206}Pb as a ^{230}Th decay product (Parrish, 1990; Schärer, 1984), was applied to all analyses of Cenozoic age. Correction of ^{206}Pb/^{238}U
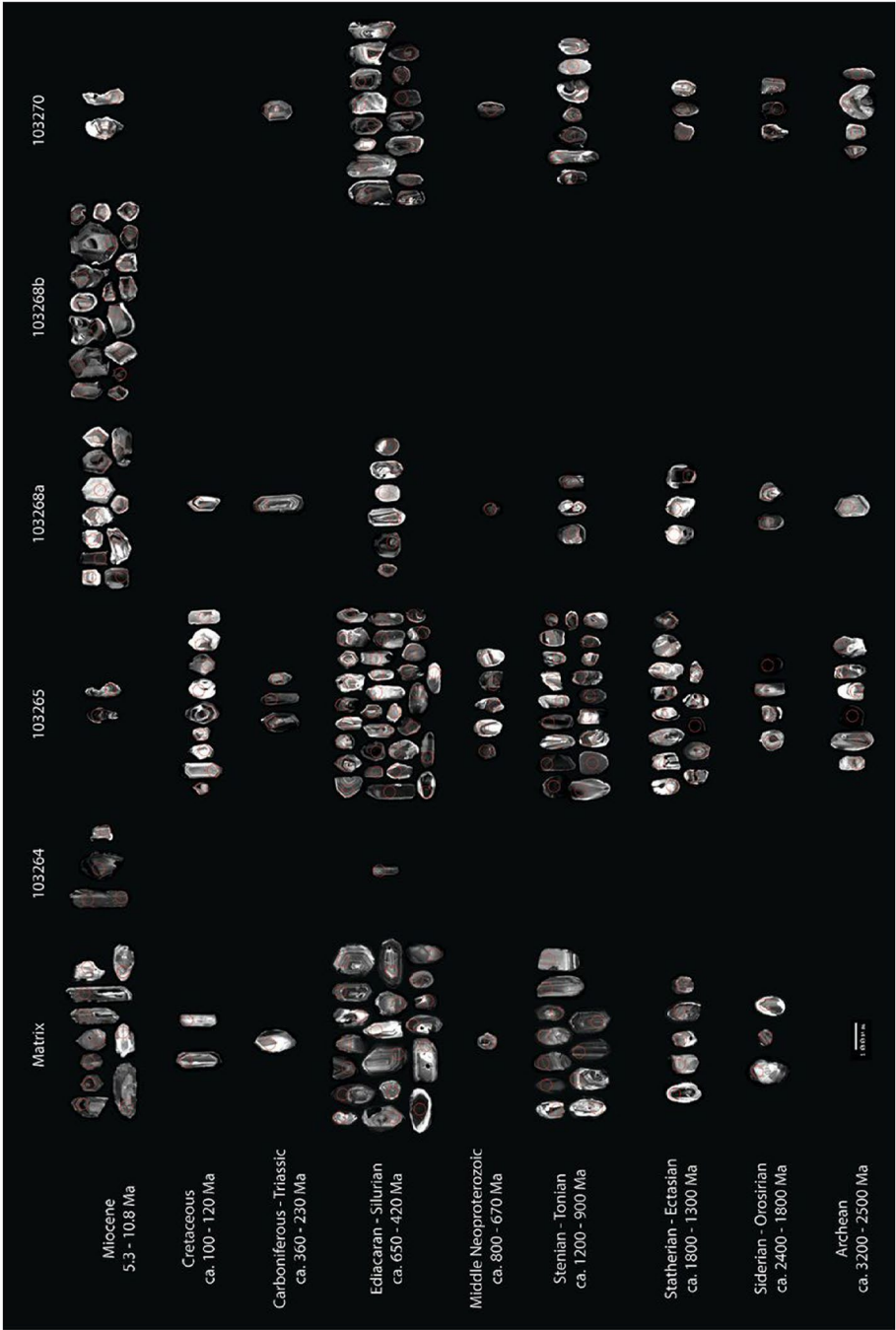
Figure 4. Cathodoluminescence for all concordant zircon grains, and grains interpreted to belong to concordant igneous populations in this study. Grains are arranged by sample and interpreted age to illustrate distribution of zircon ages and grain morphology.

Note: Red circles denote laser ablation spot locations.

ages for the ^{206}Pb deficit utilized Th and U concentrations for zircon determined during LA-ICP-MS analysis; equivalent concentrations in the melt were determined from bulk rock analysis for samples where zircons were derived from conglomerate clasts. A melt Th/U ratio of 3 ± 0.3 was assumed for zircons extracted from the matrix samples. Uncertainties associated with the correction were propagated into errors on the corrected ages according to Crowley, Schoene, and Bowring (2007). The effect of common Pb was taken into account by the use of Tera–Wasserburg Concordia plots (Jackson et al., 2004; Tera & Wasserburg, 1972). Spot ages were corrected for common Pb by utilizing the Age7Corr algorithms in Isoplot, with the isotopic common-Pb composition modeled from Stacey and Kramers (1975). Weighted mean ^{206}Pb/^{238}U age calculations were carried out using Isoplot. All errors for Cenozoic zircons were propagated at 2σ level and reported at 2σ and 95% confidence for concordia and weighted averages, respectively.

Isotopic data derived from detrital and xenocrystic zircon grains (greater than Miocene in age) were discriminated based on age. Where grain ages were in excess of 1,000 Ma, the ^{207}Pb/^{206}Pb age was preferred and assessed for discordance between the ^{207}Pb/^{206}Pb and ^{206}Pb/^{238}U age systems; while grains below 1,000 Ma in age were reported according to the ^{206}Pb/^{238}U age and assessed for discordance between ^{207}Pb/^{206}Pb and ^{206}Pb/^{238}U and ^{206}Pb/^{238}U and ^{207}Pb/^{235}U age systems. A 20% discordance threshold was used as the cut-off limit beyond which analyses were excluded from further data reduction. The preferred inherited ages taken forward for analysis were a combination of ^{207}Pb/^{206}Pb and ^{206}Pb/^{238}U ages and all errors were propagated and reported at a 1σ level; these were plotted using the cumulative probability plot and histogram function of Isoplot. A similar methodology was used for Miocene ages using a 30% discordance cut-off to provide for the increased level of uncertainty in young U–Pb ages.

Selected samples that featured a prevalence of zircons crystals underwent additional *in situ* analysis for zircon Hf isotopes. Laser ablation analyses of zircons for Lu–Hf isotope ratios were carried out at the Advanced Analytical Centre, JCU, using a GeoLas193-nmArF laser and a Thermo-Scientific Neptune multicollector ICP-MS following the setup outlined in Næraa et al. (2012) and Kemp et al. (2009). Suitable zircon crystals were selected on the basis of size and U–Pb dating results, and ablation was carried out at a repetition rate of 4 Hz and a spot size of 60 μm. All ^{176}Hf/^{177}Hf ratios for standard and sample zircons were normalized to measurements of the Mud Tank reference zircon (average measured 176Hf/177Hf ratio during this study was 0.282495 [n = 18], normalized to solution value of 0.282507) and compared with the FC1 secondary zircon standard (average 176Hf/177Hf value for this study is 0.282177, with reference to the solution value of 0.282167 ± 10; Kemp et al., 2009). Epsilon Hf values for the data were calculated following the procedure of Holm et al. (2015).

4. Results

4.1. U–Pb geochronology

All samples underwent mineral separation procedures; however, the zircon yield was highly variable for the selected sample suite. Both the volcanic nature of the rock types, and the sample size are considered contributing factors to inconsistent zircon yields. Of the nine clast samples studied, only five samples yielded zircons, and the number of zircons grains returned from the samples varied significantly (Table 2).

Results from the U–Pb zircon dating returned ages ranging from the latest Miocene–earliest Pliocene up to the Mesoarchean. These will be presented as two distinct sets of results. The first comprises ages ranging from 5.26 ± 0.27 Ma up to 14.67 ± 0.64 Ma (2σ error), broadly spanning the middle–late Miocene. These zircon crystals exhibit morphology and CL textures that are predominantly euhedral and prismatic with oscillatory zoning (Figure 4). The Th/U ratio among this suite of Miocene zircons ranges from 0.44 to 2.88 with an average of 1.41. Corresponding Tera–Wasserburg concordia and weighted average plots for these data are shown in Figure 5 and results are outlined in Table 2; we will cite the concordia ages of the samples. Sample 103264 yielded an age of 5.99 ± 0.31 Ma (n = 4), while samples 103268a and 103268b returned similar ages of 5.77 ± 0.21 Ma

(*n* = 7) and 5.71 ± 0.13 Ma (*n* = 12), respectively. Coupled with the euhedral, oscillatory-zoning CL textures (Figure 4; also see supplementary material), the relatively high U/Th ratios indicate these zircon U–Pb dating results mostly likely reflect igneous crystallization ages (e.g. Ahrens, Cherry, & Erlank, 1967; Corfu, Hanchar, Hoskin, & Kinny, 2003; Heaman, Bowins, & Crocket, 1990; Hoskin & Schaltegger, 2003). The matrix did produce a concordant zircon population that yielded an age of 8.22 ± 0.19 Ma (n = 6), however, younger zircon ages within the same sample suggest this is an in-herited magmatic age. Results for all samples passing the 30% discordance cut-off within this age suite form a distinct concentration of ages between approximately 5 and 7 Ma, and peaking at 6 Ma, with isolated ages extending back to 11 Ma (Figure 5).

Of the 267 zircon grains analyzed for this study, 185 of these (passing 20% discordance) yielded ages older than Miocene, and indeed older than Cenozoic (Figures 4 and 5), with the youngest pre-Miocene age at 99.8 ± 1.7 Ma (1σ error). Significant age populations within this data-set include a Cretaceous population that exhibit euhedral and prismatic grain morphology (Figure 4), and spans ca. 100–120 Ma (12 grains [6%]); a minor population of euhedral and prismatic zircons of Carboniferous–Triassic age (ca. 360–230 Ma) that comprises just 5 grains (3%); a broad population from the Ediacaran to the Silurian (ca. 650–420 Ma; 72 grains [39%]), with two peaks at approximately 460 Ma and 580 Ma. These zircon grains range from euhedral and prismatic with distinct oscillatory zoning to rounded grains with patchy and/or diffuse CL textures. Subsequent older zircon populations are largely comprised of rounded zircon grains with a range of CL textures (Figure 4); these include a middle Neoproterozoic population (ca. 670–800 Ma) of just 8 grains [4%]); a Stenian to Tonian Population (ca. 1200–900 Ma; 38 grains [21%]), with a significant peak at ~990 Ma, and a smaller peak at ~1120 Ma; minor populations extend back into the Mesoarchean, with peaks at ~1450, ~1630, and ~1890 Ma. The distribution of ages did not vary significantly between the zircon grains separated from the clasts and those from the matrix (Figure 5).

4.2. Major and trace elements

Major and trace element composition of clast samples are given in Table 3. Loss on ignition (LOI) values are generally moderate (2.0–3.5%), with the exception of sample 103262 at 8.2%. Geochemical compositions indicate the sampled rocks are alkaline, according to the classification of Irvine and Baragar (1971), and form a continuum with previous analyses of the Cloudy Bay Volcanics and the regional Fife Bay Volcanics (Figure 6(a); Smith, 1976). In comparison, representative analyses of the Northern Volcanic Belt of the Papuan Peninsula (see Figure 1; Smith, 1982) are distinct from the Cloudy Bay and Fife Bay Volcanics in that they are subalkaline in composition. Rock types show high variation and include basalt, trachybasalt, basaltic trachyandesite, and trachyandesite composi-tions (Figure 6; Le Maitre, 2002). The majority of these analyses also belong to the shoshonite series (Figure 6(b)) and are predominantly distributed across both the absarokite and shoshonite composi-tional fields of Peccerillo and Taylor (1976).

Major element variation diagrams (Figure 7) have been used to show geochemical trends for clasts derived from the Cloudy Bay Volcanics, together with previous analyses of the Cloudy Bay Volcanics and the Fife Bay Volcanics (Smith, 1976). SiO_2 contents of samples from this study (nor-malized for volatile-free compositions) vary from 48 to 56 wt.% (45 to 55 wt.% as measured), and MgO vary from approximately 8.5 to 3 wt.%. This range is similar to previous analyses of the Cloudy Bay Volcanics (48 wt.% < SiO_2 < 61 wt.%; 1 wt.% < MgO < 9 wt.%) and generally reflect more evolved compositions when compared to the Fife Bay Volcanics (47 wt.% < SiO_2 < 56 wt.%; 3 wt.% < MgO < 14 wt.%). The major elements Fe_2O_3 and CaO, together with MnO exhibit a good positive correlation with MgO (or negative with SiO_2), whereas Al_2O_3, K_2O, and TiO_2 show negative correlations with MgO. A similar, but weaker, negative correlation is evident between Na_2O and MgO. The major element data presented here, together with previous results from the Cloudy Bay Volcanics and the Fife Bay Volcanics, appear to form a compositional continuum.

Table 2. Zircon U–Pb geochronology results

Sample	Number of analyses	Miocene ages[a]	> Miocene ages[b]	Youngest age[a]	1σ Error	Concordia age	2σ Error	MSWD	Probability of fit	Weighted average	95% Confidence	MSWD	Probability of fit	N
Matrix	63	7	42	5.3	0.1	8.22[c]	0.2	1.5	0.19	8.18[c]	0.22	1.3	0.26	6
103264	6	4	1	6.0	0.1	5.99	0.3	0.07	0.93	6.09	0.13	0.2	0.89	4
103265	103	2	90	5.5	0.1									
103268a	36	11	18	5.7	0.1	5.77	0.2	0.56	0.73	5.92	0.15	2.2	0.043	7
103268b	19	17	0	5.4	0.1	5.71	0.1	1.2	0.28	5.82	0.06	1.5	0.14	12
103270	40	2	34	5.3	0.1									

[a]Ages passing 30% discordance cut-off.

[b]Ages greater than Miocene passing 20% discordance cut-off.

[c]Representative of an inherited magmatic age.

Figure 5. Zircon U–Pb dating results for the Cloudy Bay Volcanics. Tera–Wasserburg concordia and weighted average are constructed from zircon isotopic compositions and U–Pb calculated ages, respectively (detailed isotopic data in supplementary material). Tera–Wasserburg plots are corrected for initial Th disequilibrium; weighted average plots are corrected for initial Th disequilibrium and $^{207}Pb/^{206}Pb$ common Pb. All error bars, data point error ellipses and calculated errors are 2σ and 95% confidence for concordia and weighted averages, respectively. Probability–density histograms are shown for concordant grains, with Miocene ages <30% discordance and greater than >Miocene (pre-Cenozoic) ages <20% discordance.
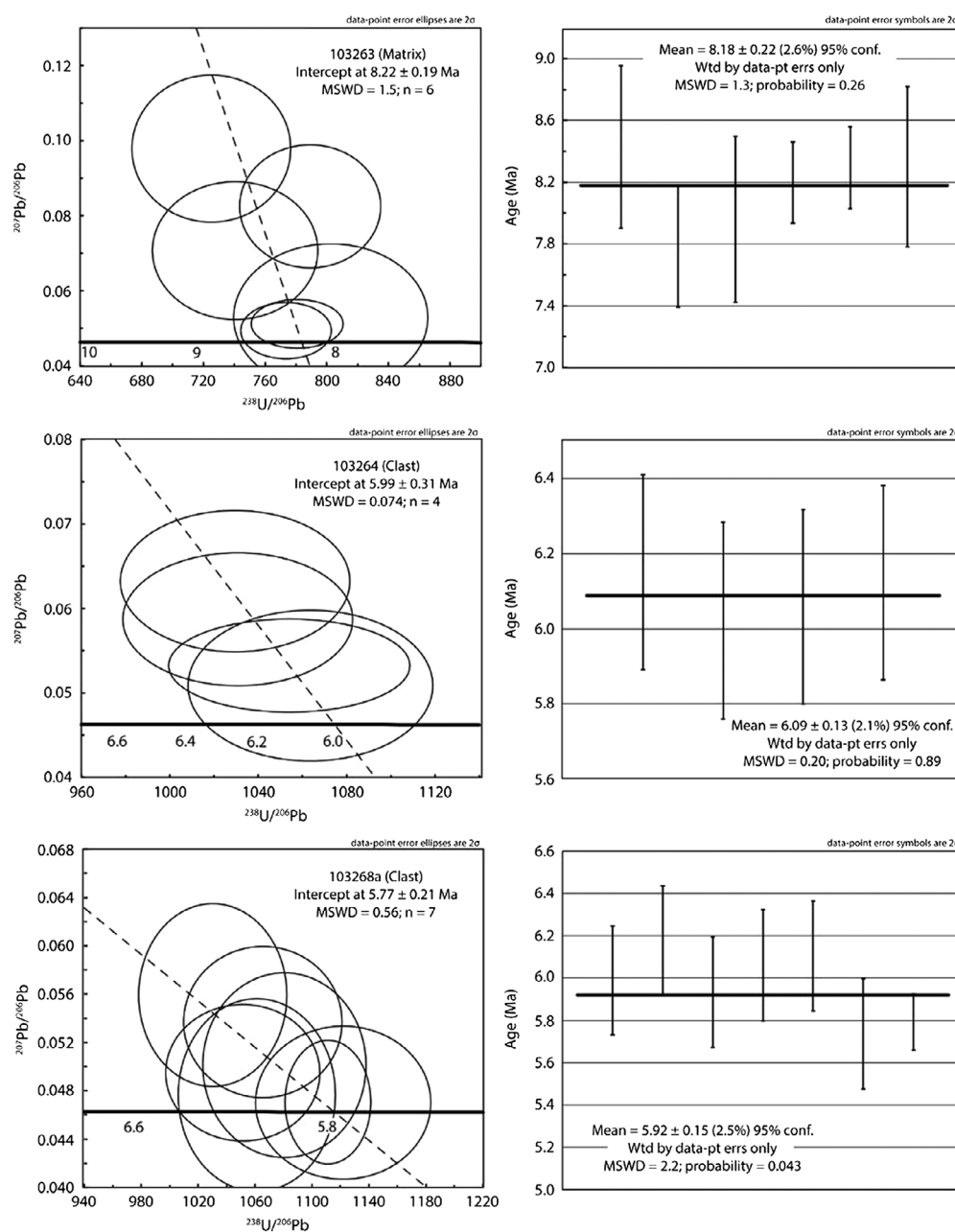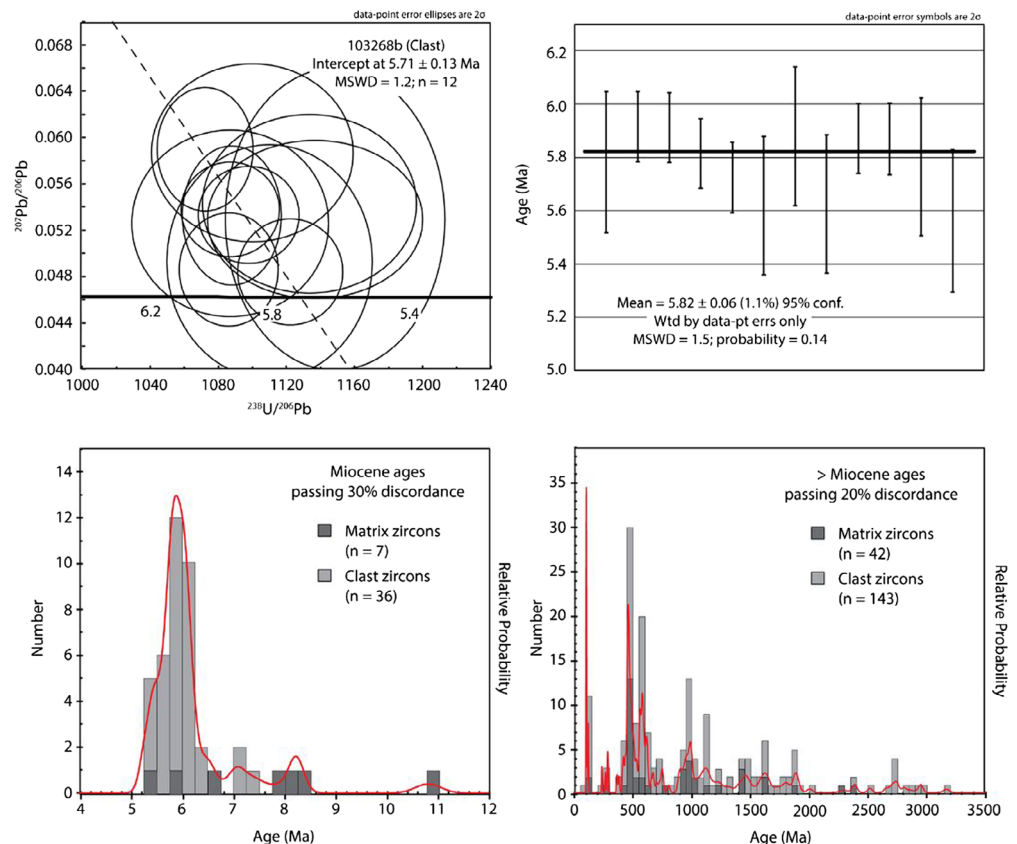
Figure 5. (*Continued*)

Trace element data are presented in Figure 8 by way of normalized multi-element plots and *X–Y* plots. All samples from the Cloudy Bay Volcanics exhibit subduction-related geochemical affinities (Figure 8(a)) with negative Nb, Ta, and Ti anomalies, and relative enrichments in large-ion lithophile elements (LILE), Th, U, Pb, and Sr. On comparison with previous analyses (Figure 8(b)), the results presented herein correlate well with prior results of the Cloudy Bay Volcanics from Smith (1976). Weathering and alteration has affected the samples to varying extents; we will therefore, not focus on the LILE (e.g. K, Rb, Cs) or Sr in detail as these elements are easily mobilized during alteration and will instead focus more on the less mobile HFSE (Nb, Ti, Zr, Hf), REE, and Th (e.g. Floyd & Winchester, 1978). All samples exhibit light REE-enriched patterns (Figure 8(c)) that are typical of evolved subduction-related magmas. The sample suite generally appears to form a compositional continuum with different degrees of light REE enrichment. This is supported by, for example, Figure 8(d) that demonstrates a positive correlation between the slope of the REE trend and Nb, and similarly Zr concentrations (Figure 8(f)). There are minor differences, however, where samples 103265, 103267, 103268c, and 103269 are generally characterized by lower light REE abundances in comparison to samples 103264, 103268a, 103268b, 103268d, and 103270. The latter suite of samples also exhibits minor negative Eu anomalies and REE trends more consistent with heavy REE depletion (Figure 8(c)). Differences in the two sample suites are also evident in plots of Y (Figure 8(e) and (g)), where two different correlation trends are apparent. That is, samples 103264, 103268a, 103268b, 103268d, and 103270 are marked by heavy REE-depleted trends, and exhibit a relative *Y*-depletion, compared to the remainder of the samples. These characteristics of variable *Y* contents also distinguish previous analyses of the Cloudy Bay Volcanics from the Fife Bay Volcanics (Figure 8(g)).

Table 3. Representative major and trace element data

Sample	103264	103265	103267	103268a	103268b	103268c	103268d	103269	103270
SiO_2	51.39	45.01	47.19	52.31	52.66	48.15	51.37	54.59	52.21
Al_2O_3	14.76	14.45	13.9	16.48	15.83	15.25	15.56	17.19	14.31
Fe_2O_3	8.5	11.1	9.87	8.97	8.92	10.5	9.37	7.42	8.34
MgO	4.83	7.34	8.35	2.97	3.23	5.62	3.94	2.86	4.63
CaO	8.11	8.51	10.56	5.3	5.16	10.1	6.74	5.8	7.93
Na_2O	3.45	1.44	2.05	2.76	2.25	3.35	3.49	3.77	3.99
K_2O	3.04	1.17	3.66	5.11	6.66	1.09	2.99	4.14	2.95
TiO_2	1.2	1.02	0.92	1.26	1.21	1.1	1.3	0.74	1.16
P_2O_5	0.93	0.91	0.76	0.91	0.86	0.77	1.01	0.54	0.89
MnO	0.15	0.21	0.16	0.11	0.13	0.15	0.13	0.08	0.15
Cr_2O_3	0.01	0.068	0.038	0.019	0.017	0.004	0.01	0.013	0.009
LOI	2.9	8.2	2	3.3	2.6	3.4	3.4	2.5	2.8
Total	99.54	99.7	99.59	99.68	99.73	99.7	99.55	99.77	99.55
Sc	21	32	27	22	21	28	22	15	20
V	229	253	263	239	107	309	198	149	223
Co	22.6	45.5	36	28.7	23.2	31.7	23.7	17.2	22.2
Ni	59	107.3	61.5	67.4	19.2	58.9	48.8	28.6	32.4
Cu	78.6	116.5	120.3	75.1	28.1	110.2	53.9	51.2	72.6
Zn	80	51	66	80	20	75	51	37	75
Ga	18.5	14.9	15.4	20.6	18.8	17.1	19.7	17	18.3
As	1.3	1	1	1	6.2	0.5	1.5	2.1	1.8
Rb	35.7	34	324.5	184.4	273.1	81.7	36.3	197.5	64.9
Sr	1855	680.5	1476	1288.7	1158.4	900	1905.4	927.5	1890.3
Y	28.8	20.7	14.3	19.3	16.7	19.6	23.1	24.1	27.5
Zr	399.9	85.7	81.9	224.9	212.2	89.4	407.3	133.7	384.9
Nb	12.7	3	3.1	7.8	7.1	3.4	13.8	4.5	12.6
Mo	0.2	0.3	0.7	0.5	0.3	1.1	0.3	0.8	0.3
Sn	6	2	1	3	4	1	6	1	6
Cs	29.2	1	7.6	3.1	1.7	57.7	1.2	3.4	63.4
Ba	1950	2018	780	1681	1560	2511	1961	918	2032
La	50.8	16.7	13.8	34.6	31.6	11.6	49.7	19.7	49.6
Ce	107	36.3	27.8	71.7	70	24.4	103.2	34.4	104.5

(*Continued*)

Table 3. (Continued)

Sample	103264	103265	103267	103268a	103268b	103268c	103268d	103269	103270
Pr	14.26	5.07	3.94	9.78	8.8	3.83	13.64	5.61	14.09
Nd	58.2	22.5	17.8	39.8	34.9	17.7	53.6	22.9	57.3
Sm	11.35	4.84	3.74	7.88	6.97	4.08	9.99	4.87	10.89
Eu	2.8	1.57	1.23	2.06	1.78	1.36	2.57	1.57	2.76
Gd	9.22	4.89	3.47	6.5	5.71	4.16	7.89	4.96	8.83
Tb	1.16	0.68	0.48	0.83	0.73	0.63	1.03	0.69	1.15
Dy	5.93	4.08	2.8	4.24	3.64	3.61	4.81	3.9	5.61
Ho	1	0.77	0.5	0.71	0.64	0.73	0.85	0.82	0.98
Er	2.59	2.14	1.39	1.87	1.62	2.02	2.14	2.26	2.64
Tm	0.35	0.31	0.19	0.25	0.21	0.28	0.29	0.3	0.33
Yb	2.11	1.87	1.13	1.5	1.27	1.81	1.73	1.93	2.07
Lu	0.32	0.28	0.17	0.23	0.19	0.29	0.25	0.3	0.33
Hf	11.2	2.6	2.4	6.1	5.9	2.6	11.5	3.5	10.8
Ta	0.7	0.2	0.2	0.4	0.5	0.3	0.9	0.3	0.8
W	0.9	<0.5	0.6	0.6	0.8	<0.5	2	2.6	1.5
Tl	0.2	0.3	0.6	0.2	<0.1	0.2	<0.1	<0.1	0.5
Pb	2.9	5.6	12	6.5	5.7	2	6.6	5.8	4.2
Th	24.8	4.3	4.1	16	14.9	2.6	26.3	6.9	25.3
U	7.2	0.8	1.6	4.6	3.4	1	7.7	2.4	7.3

Figure 6. (A) Total alkali versus silica classification diagram (TAS; Le Maitre, 2002) with alkaline–subalkaline curve of Irvine and Baragar (1971), and (B) K₂O vs. SiO₂ diagram of Peccerillo and Taylor (1976). Additional data from previous analyses of the Cloudy Bay Volcanics, Fife Bay Volcanics, and the Northern Volcanic Belt is from ¹Smith (1976) and ²Smith (1982). Data is normalized and plotted on a volatile-free basis.
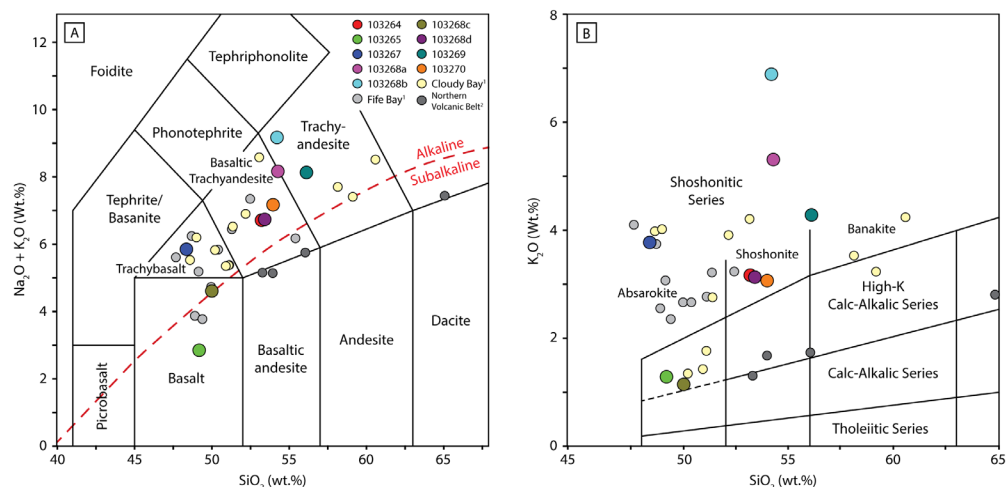
4.3. Lu–Hf isotopes

Selected zircons from samples 103263 (matrix), 103264, 103268a, and 103268b were analyzed for Lu–Hf isotopic ratios. The zircon crystals selected for this additional analysis were chosen to provide a representative range of ages across the sample suite as established by U–Pb dating. The results are reported in Table 4 and illustrated in Figure 8(h). All εHf values fall within a range between +11.1 and +6.9. However, there are distinct ranges for εHf values that correlate with the zircon U–Pb ages. Although only a single analysis, the oldest zircon grain at ca. 10.8 Ma yielded the second most mantle-like εHf value of +10.7; a second cluster comprising three analyses ranging between 8.3 and 8.0 Ma in age yielded an average εHf value of +10.2. The majority of analyzed zircons fall within the age range of 6.4–5.5 Ma and provided a range of εHf values between +9.8 and +6.9, with a corresponding average εHf value of +7.9.

5. Discussion

5.1. Petrology of the Cloudy Bay volcanics derived from a conglomerate

Up to nine variations of volcanic rocks were identified as clasts derived from a secondary conglomerate deposit and interpreted as an erosional product of the Cloudy Bay Volcanics. The volcanic rocks exhibit variable textures ranging from volcanic glass to porphyritic lavas and represent a compositional continuum from basalt to trachyandesite. The geochemical results derived from the conglomerate clasts outlined above are consistent with previous studies of regional late Miocene to Recent arc-type volcanic activity, which comprises a variety of high-K calc-alkaline rocks and volcanic–plutonic shoshonite suites (Jakeš & Smith, 1970; Smith, 1972, 1982, 2013b; Smith & Milsom, 1984).

The geochemical investigations of the Cloudy Bay Volcanics presented herein support previous interpretations that the volcanics are derived from partial melting of subduction-modified mantle in a volcanic arc setting (Figure 8). As the context of the outcrop is not conclusively constrained within the Cloudy Bay Volcanics and does suffer from a moderate degree of weathering and alteration, we will not focus here on detailed petrogenesis of the volcanics. Instead, we will emphasize the geochemical indicators relevant to wider scale studies of tectonics and crustal processes. We find that the sample suite generally reflects a compositional continuum, but with minor distinctions that suggest the potential for different magma evolution pathways. We interpret that the volcanic rock clasts can be divided into two sample suites on the basis of REE trends correlated with differential *Y* contents. We refer to samples 103265, 103267, 103268c, and 103269 as Suite 1, comprising basalts, a trachybasalt, and one trachyandesite. Suite 2 includes samples 103264, 103268a, 103268b, 103268d, and 103270, and comprises basaltic trachyandesites and trachyandesites. Although subtle, differences in REE trends of Suite 2 rocks, in comparison with Suite 1, provide evidence of an

Figure 7 Major element variation diagrams. Additional data from previous analyses of the Cloudy Bay Volcanics, Fife Bay Volcanics, and the Northern Volcanic Belt is from [1]Smith (1976) and [2]Smith (1982). Data are normalized and plotted on a volatile-free basis.
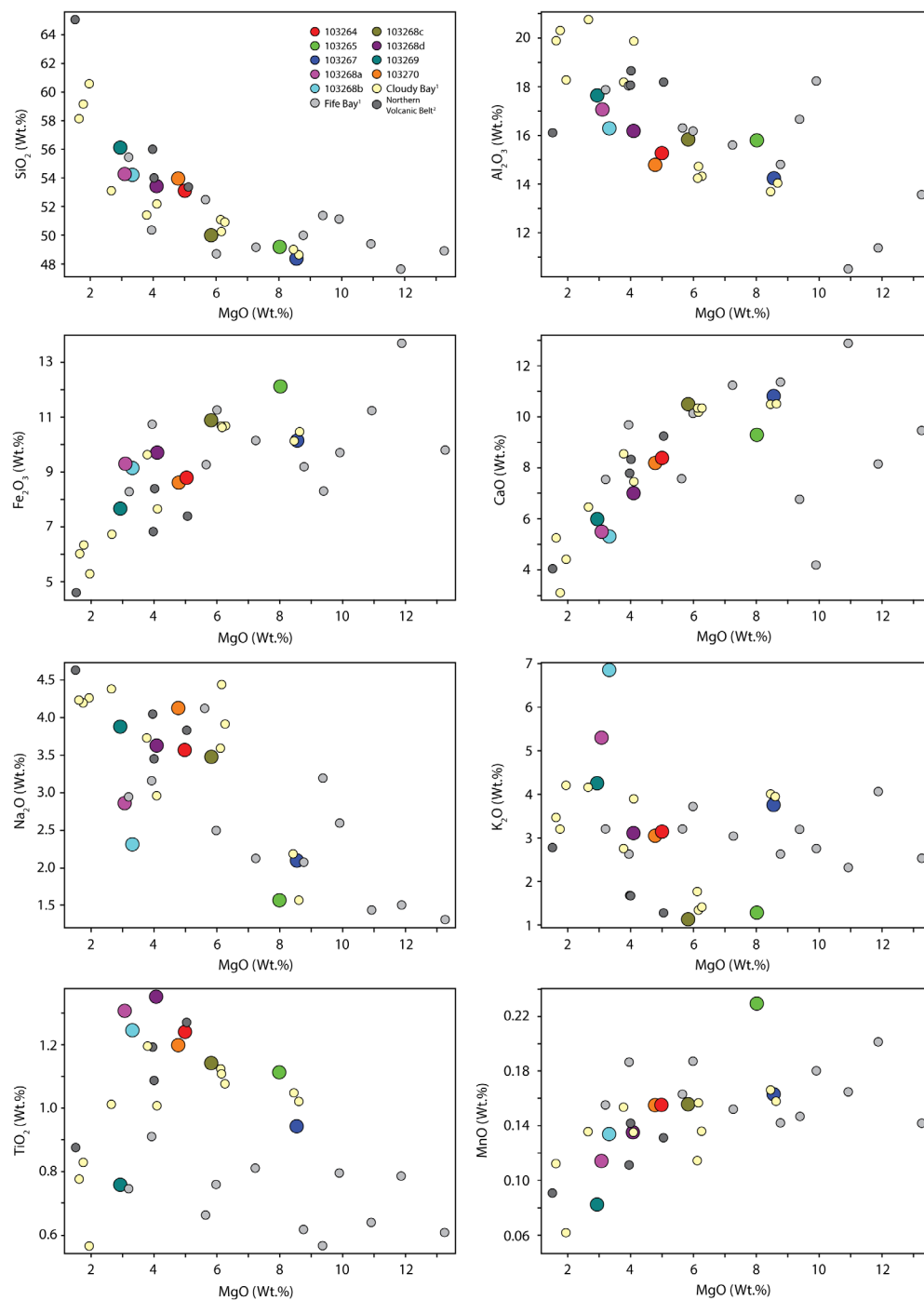
Figure 8. (A) N-MORB normalized multi-element plot; (B) N-MORB normalized multi-element plot for average compositions for samples from this study, and previous analyses from Cloudy Bay and Fife Bay ([1]Smith, 1976); (C) C1 chondrite normalized REE plots for the Cloudy Bay Volcanics. N-MORB and C1 chondrite normalizations are from Sun and McDonough (1989). (D)–(G) Trace element X–Y scatter plots, and (H) Zircon εHf (t) values for zircons of the Cloudy Bay Volcanics; crosses are 1σ errors.
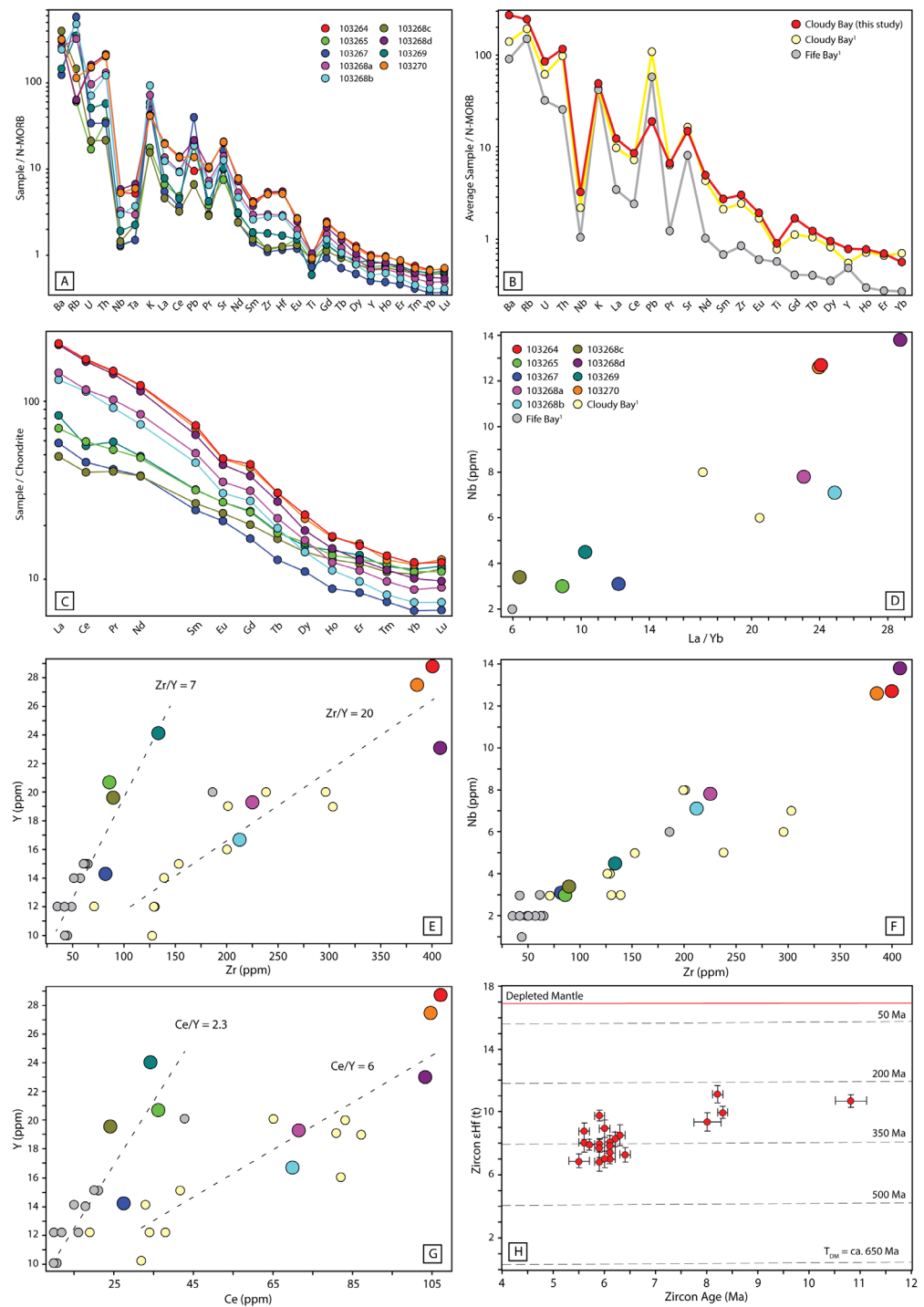
Table 4. Lu–Hf isotope data.

Sample	Spot ID	U–Pb Spot Age (Ma)	±1σ	^{176}Hf/^{177}Hf	±1σ	^{176}Lu/^{177}Hf	±1σ	εHf (t = age)	±1σ
103263	21	10.8	0.3	0.283081	0.000012	0.001971	0.000007	10.7	0.4
	23	8.3	0.1	0.283062	0.000011	0.001206	0.000010	10.0	0.4
	27	8.2	0.1	0.253095	0.000016	0.006811	0.000091	11.1	0.6
	31	8.0	0.3	0.283045	0.000016	0.002608	0.000074	9.4	0.6
103264	2	6.1	0.1	0.282991	0.000014	0.001816	0.000014	7.4	0.5
	5	6.1	0.1	0.283010	0.000012	0.001316	0.000025	8.1	0.4
103268a	1	6.0	0.1	0.282979	0.000015	0.001840	0.000034	7.0	0.5
	15	6.2	0.1	0.283015	0.000013	0.001303	0.000029	8.3	0.5
	19	5.9	0.1	0.283000	0.000017	0.001765	0.000025	7.7	0.6
	20	6.1	0.1	0.282980	0.000009	0.001678	0.000016	7.0	0.3
	27	6.1	0.1	0.283003	0.000008	0.001458	0.000022	7.8	0.3
	33	6.4	0.1	0.282987	0.000013	0.001780	0.000015	7.3	0.4
	36	6.3	0.1	0.283022	0.000019	0.002961	0.000064	8.5	0.7
103268b	2	5.9	0.1	0.283007	0.000009	0.001611	0.000014	8.0	0.3
	3	5.9	0.1	0.283058	0.000010	0.001513	0.000014	9.8	0.3
	5	5.7	0.1	0.283005	0.000010	0.001193	0.000008	7.9	0.3
	6	6.0	0.1	0.283035	0.000015	0.001620	0.000007	9.0	0.5
	7	5.6	0.1	0.283010	0.000017	0.001693	0.000019	8.1	0.6
	9	5.6	0.1	0.283030	0.000014	0.001944	0.000030	8.8	0.5
	10	5.9	0.1	0.283075	0.000018	0.001771	0.000030	6.9	0.6
	18	5.5	0.2	0.283077	0.000012	0.001517	0.000074	6.9	0.4

increased level of fractionation, with more pronounced light REE enrichment and negative Eu anomalies. These characteristics are attributed to plagioclase fractionation, and typical of high-K calc-alkaline magmas (Gill, 1981). Samples belonging to Suite 2 also exhibit heavy REE- and *Y*-depletion, which are both typically linked to magma that has undergone fractionation of garnet at high pressures in the upper mantle or lower crust (Chiaradia, Merino, & Spikings, 2009; Macpherson, Dreher, & Thirlwall, 2006). We also observe that in general, Suite 2 samples are also more fractionated in that they are marked by higher relative SiO_2, K_2O, and TiO_2 concentrations compared with Suite 1 samples (Figure 7), and lower MgO, FeO, and CaO concentrations. We therefore interpret that the sample suite represents a geochemical compositional continuum of shoshonitic volcanics, but that different magma evolution pathways are apparent within the sample suite. That is, Suite 2 volcanic rocks have undergone additional magma fractionation under high-pressure conditions.

Zircon U–Pb dating results from the clast samples indicate that activity of the Cloudy Bay Volcanics was largely constrained to the latest Miocene–earliest Pliocene, at between ca. 7 and 5 Ma in age. Zircon dating also provides evidence for magmatism in the area as old as 11 Ma, but it is not clear if this is related to an earlier phase of volcanic activity or is inherited and belongs to a separate suite of magmatism. The Cloudy Bay Volcanics were previously inferred to be of equivalent age to the Fife Bay Volcanics (Figure 1), dated at 12.6 Ma (Smith & Davies, 1976; Smith & Milsom, 1984); high-K basalts of Woodlark Island, dated at 11.2 Ma (Ashley & Flood, 1981; Smith & Milsom, 1984); and plutons and dykes swarms that intrude the eastern Milne Basic Complex, and dated at 16–12 Ma (Smith, 1972; Smith & Milsom, 1984). Given the revised age for the Cloudy Bay Volcanics, this volcanic activity should now be associated with a later generation of regional volcanism, namely andesites and shoshonites north of, and adjacent to the D'Entrecasteaux islands, dated at 5.5 Ma, and a granite intrusive complex at Mt Suckling dated at 6.3 Ma (Smith & Davies, 1976; Smith & Milsom, 1984).

This study also presents the first Lu–Hf isotope results from the Papuan Peninsula. The Hf isotope results are derived from zircons belonging to volcanic rocks of Suite 2 and the outcrop matrix, and as a result we cannot draw any conclusions about differences between the two geochemical suites. Instead, we interpret these results within the context of the regional tectonics. The Hf results display a tight range of εHf values between +9.8 and +6.9 for the majority of the sampled zircons indicating a relatively homogonous magma composition (Figure 8(h)). The εHf values are much less positve than would be anticipated from Miocene–Pliocene mantle-derived basaltic melts, which is interpreted to reflect contamination of the magma by comparavtively unradiogenic crust. The corresponding depleted mantle model age for the same εHf values of ~200–400 Ma does provide comfirmation that older crustal material has contributed to the magma composition, but given the complex mixing and assimilation processes in arc magmatism we place little emphasis on the precise model ages. We do note that the apparent decrease in εHf values and associated model age (Figure 8(h)) over time may reflect either a changing source or an increase in the degree of assimilation and mixing with foreign crustal material.

Potential sources of crustal contamination will arise from either the melt source region in the mantle, or lithospheric crust through which the magma has migrated. Rocks of the Milne Terrane can provide a first pass proxy for the upper crustal material in the vicinity of Cloudy Bay. These are comprised largely of Upper Cretaceous N-MORB-type basaltic volcanics (Smith, 2013a); such primative rocks are unlikely to yield sufficiently unradiogenic crustal signatures to yield the Lu–Hf ratios reported herein, however, this requires further work. An alterative isotopic source that must be considered is the crust of the Eastern and Papuan Plateaus to the south of the Papuan Peninsula. The geology of the plateaus is not clear at present, however, the Queensland Plateau forming the congugate southern margin of the Coral Sea has been previously interpreted to form part of the New England Orogen of Eastern Australia (Mortimer, Hauff, & Calvert, 2008; Shaanan, Rosenbaum, Hoy, & Mortimer, 2018). Although far removed from the context of the present study, previous Hf isotope data from the southern New England Orogen has provided εHf values ranging from +3.4 to +11.3 (Kemp et al., 2009). While this is speculative at this stage we infer that underthrust portions of the

Eastern and Papuan Plateau beneath the Papuan Peninsula related to past convergent events do have the potential to contribute to magma genesis and could go someway to explaining the Lu–Hf isotope ratios of the Cloudy Bay Volcanics.

The newly established timing for activity of the Cloudy Bay Volcanics, the recognition of multiple magma evolution pathways with similar ages, and the interpretation for the involvement of comparatively unradiogenic crust are important contributions in the context of the regional tectonic evolution of Papua New Guinea. The middle Miocene to early Pliocene is a time of tectonic upheaval, marked by middle to late Miocene closure of the Pocklington trough and development of the New Guinea Orogen related to collision of the Australian continent (Cloos et al., 2005; Holm et al., 2015; Webb, Baldwin, & Fitzgerald, 2014), thickened arc crust (Drummond, Collins, & Gibson, 1979; Milsom & Smith, 1975), and interpreted lithospheric delamination beneath the Papuan Highlands from ca. 6 Ma (Cloos et al., 2005; Holm et al., 2015); delamination has similarly been interpreted beneath the Papuan Peninsula (Abers & Roecker, 1991; Eilon, Abers, Gaherty, & Jin, 2015). Early Pliocene regional tectonics are marked by the onset of rifting and sea floor spreading in the Woodlark Basin from at least 5 Ma (Holm, Rosenbaum, & Richards, 2016; Taylor, Goodliffe, & Martinez, 1999; Taylor, Goodliffe, Martinez, & Hey, 1995; Wallace et al., 2014), Pliocene subduction of the Solomon Sea plate at the Trobriand trough (Holm et al., 2016), and late Miocene to Recent formation of the Aure–Moresby fold–thrust belt (Ott & Mann, 2015). An in-depth interpretation of the tectonic context for activity of the Cloudy Bay Volcanics is beyond the scope of this study, however, ongoing work on the tectonic and magmatic evolution of the Papuan Peninsula will aim to provide greater insights into the dynamic regional setting.

5.2. Provenance of zircon xenocrysts

The majority of zircon grains recovered from the sampled clasts and matrix material are of pre-Cenozoic age (Figures 4 and 5) and represent xenocrystic zircon grains inherited from a foreign source. There are two possible mechanisms to explain the presence of inherited zircons within the Cloudy Bay Volcanics. The first appeals to assimilation of older crustal basement into the magma during migration and ascent through the crust. Alternatively, the grains may have been present at the Earth's surface, for example within fluvial systems, and subsequently incorporated into the rocks during subaerial volcanism. Sample petrography does not identify any notable component of xenoliths or xenocrysts that could be considered as surface material during eruption and cooling. We therefore suggest that the xenocrystic zircon grains were introduced to the magma via assimilation of crustal basement (e.g. Buys, Spandler, Holm, & Richards, 2014; Paquette & Le Pennec, 2012; Van Wyck & Williams, 2002).

The geological setting of the Papuan Peninsula at the present day, and similarly throughout the late Cenozoic, is bound by oceanic basins to the north and south (e.g. Hall, 2002; Holm et al., 2015, 2016; Schellart, Lister, & Toy, 2006), and precludes the introduction of zircons from distal crustal sources into the Papuan Peninsula setting leading up to the late Miocene volcanism. Instead, the presence of inherited or detrital zircons within the Cloudy Bay Volcanics requires assimilation of older basement crust (e.g. Buys et al., 2014; Paquette & Le Pennec, 2012; Van Wyck & Williams, 2002). As outlined above, the greater Papuan Peninsula is comprised or, or underlain by the Owen Stanley Metamorphic Complex and Milne Terrane (Davies, 2012; Smith, 2013a), the protolith of which is interpreted to be largely made up of sedimentary detritus derived from middle Cretaceous felsic magmatism (Davies, 2012) and Upper Cretaceous basaltic magmatism (Smith, 2013a). Although only a minor xenocrystic population, the youngest xenocrystic zircons are middle Cretaceous in age. The youngest grain, at ca. 100 Ma, correlates well with the interpreted Albian–Cenomanian depositional age for the protolith of the Owen Stanley Metamorphic Complex (Dow et al., 1974; Kopi et al., 2000). The rocks of the Owen Stanley Metamorphic Complex, therefore, represent the most likely source for the xenocrystic zircons within the Cloudy Bay Volcanics. The abraded and rounded morphology of the majority of pre-Cretaceous zircon grains, however, indicate they are detrital in origin and do not originate from Papuan Peninsula per se (Figure 4). And by proxy, evaluation of the xenocrystic zircons can be interpreted to reflect the detrital provenance of the Owen Stanley

Metamorphic Complex (e.g. Buys et al., 2014; Fergusson, Henderson, & Offler, 2017; Paquette & Le Pennec, 2012; Van Wyck & Williams, 2002).

The xenocryst/detrital zircon record presented here is comparable to established zircon records from the eastern highlands of Papua New Guinea (Van Wyck & Williams, 2002), and recent studies from offshore of northeast Australia from the Solomon Islands (Tapster, Roberts, Petterson, Saunders, & Naden, 2014), New Caledonia (Adams, Cluzel, & Griffin, 2009; Pirard & Spandler, 2017) and Vanuatu (Buys et al., 2014). Similar to these regional studies, the pre-Cretaceous zircon populations within the Cloudy Bay Volcanics are characterized by Ediacaran to Silurian (ca. 650–420 Ma) and Mesoproterozoic to early Neoproterozoic (~1600–900 Ma) populations. Drawing from previous interpretations, these detrital age signatures are consistent with detritus that was likely sourced from recycling of basins on the eastern margin of Gondwana. These sources include the Mossman, Thomson, New England, and Lachlan Orogens of eastern Australia, of which Ordovician and Mesoproterozoic zircons form a significant component (Fergusson et al., 2017; Henderson, 1986; Pell, Williams, & Chivas, 1997; Van Wyck & Williams, 2002), and also the Charters Towers Province, and the Georgetown and Coen Inliers of northern Queensland, where major crust-forming events occurred at ca 1.55 Ga, 420–400 Ma, and 300–284 Ma (Blewett & Black, 1998; Fergusson, Henderson, Fanning, & Withnall, 2007; Fergusson, Henderson, Withnall, & Fanning, 2007; Fergusson et al., 2017; Pell et al., 1997).

An important distinction can, however, be drawn between the established zircon provenance from northeast Australia and related South West Pacific terranes, and the Cloudy Bay Volcanics. Namely, this is the absence of a significant Carboniferous–Permian zircon population that is characteristic of the Kennedy Igneous Association (330–270 Ma; Champion & Bultitude, 2013), and the main phase of the Hunter-Bowen Orogeny in the New England Orogen (Korsch et al., 2009). Regional reconstructions (e.g. Schellart et al., 2006; Tapster et al., 2014; Whattam, Malpas, Ali, & Smith, 2008) imply that during the Cretaceous, and prior to the opening of the Coral Sea, the Papuan Peninsula was located adjacent to northeast Queensland forming a continuation of the extended continental crust. Given the importance of this regional crust-forming event and the prevalence of reworked zircons related this time period in other regional terranes (e.g. Kubor and Bena Bena Blocks, eastern Papuan Highlands [Van Wyck & Williams, 2002]; Espiritu Santo, Vanuatu (Buys et al., 2014); New Caledonia (Adams et al., 2009; Pirard & Spandler, 2017), it is unusual that zircons of this age only form a minor population (3%) of the total xenocrystic zircon yield. This implies that erosion of these Carboniferous–Triassic rocks did not contribute significant volumes of material to form the sedimentary protolith of the Owen Stanley Metamorphic Complex. And furthermore, that either a barrier was in place that prevented transport of sedimentary material to the Owen Stanley terrane prior to break-up of eastern Gondwana and opening of the Coral Sea, or that reconstructions of the Owen Stanley terrane are incorrect. These results are not yet conclusive and ongoing research is underway to expand the scope of investigations into the volcanics and provenance of the Papuan Peninsula, but it does suggest that regional provenance models and tectonic reconstructions for eastern Gondwana may require revision.

6. Conclusions

We present an investigation into the petrology of the Cloudy Bay Volcanics of the southeast Papuan Peninsula, Papua New Guinea. However, this study is distinct in that we sample clasts derived from an isolated conglomerate outcrop within a region comprising dense lowland tropical forest with regional swamp forest and mangroves. Tropical regions such as this are characterized by enhanced weathering and erosion, where our ability to examine the geological record can become compromised by the absence of informative *in situ* geological outcrops. Our findings suggest that the Cloudy Bay Volcanics were largely active during the latest Miocene, between 7 and 5 Ma. The shoshonitic volcanics largely form a geochemical continuum in overall composition but form two distinct suites reflecting different magma evolution pathways. Evidence for this arises from disparate REE trends, with an anomalous volcanic suite marked by heavy REE- and Y-depletion indicative of high-pressure magma fractionation. Inclusion of a considerable number of xenocrystic zircons within the Cloudy

Bay Volcanics provide additional insights into the nature of the Owen Stanley Metamorphic Complex and Milne Terrane, which form the basement of the Papuan Peninsula, and suggests an eastern Gondwana provenance for detrital zircons. The results of this study illustrate that in such areas, characterized by incomplete data-sets and difficulties in reconciling the regional geological history, we can still gain insight into the geology by sampling of secondary deposits.

Author details
Robert J. Holm[1,2]
E-mail: rholm@frogtech.com.au
ORCID ID: http://orcid.org/0000-0001-5470-2612
Benny Poke[3]
E-mail: bpoke@mra.gov.pg
[1] Frogtech Geoscience, 2 King Street, Deakin West ACT 2600, Australia.
[2] Geosciences, College of Science & Engineering, James Cook University, Townsville, Queensland 4811, Australia.
[3] Geological Survey Division, Mineral Resources Authority, PO Box 1906, Port Moresby 121, Papua New Guinea.

References
Abers, G. A., & Roecker, S. W. (1991). Deep structure of an arc-continent collision: Earthquake relocation and inversion for upper mantle P and S wave velocities beneath Papua New Guinea. *Journal of Geophysical Research: Solid Earth, 96*, 6379–6401. https://doi.org/10.1029/91JB00145

Adams, C. J., Cluzel, D., & Griffin, W. L. (2009). Detrital zircon ages and geochemistry of sedimentary rocks in basement Mesozoic terranes and their cover rocks in New Caledonia, and provenances at the Eastern Gondwanaland margin. *Australian Journal of Earth Sciences, 56*, 1023–1047. https://doi.org/10.1080/08120090903246162

Ahrens, L. H., Cherry, R. D., & Erlank, A. J. (1967). Observations on the Th-U relationship in zircons from granitic rocks and from kimberlites. *Geochemica et Cosmochimica Acta, 29*, 711–716.

Amante, C., & Eakins, B. W. (2009). *ETOPO1 1 arc-minute global relief model: Procedures, data sources and analysis*. Silver Spring: NOAA Technical Memorandum NESDIS NGDC-24. National Geophysical Data Center, NOAA.

Ashley, P. M., & Flood, R. H. (1981). Low-K tholeiites and high-K igneous rocks from Woodlark Island, Papua New Guinea. *Journal of the Geological Society of Australia, 28*, 227–240. https://doi.org/10.1080/00167618108729158

Australian Bureau of Mineral Resources. (1972). *Geology of Papua NewGuinea, 1:1,000,000 map*. Australian Bureau of Mineral Resources.

Baldwin, S. L., Fitzgerald, P. G., & Webb, L. E. (2012). Tectonics of the New Guinea Region. *Annual Review of Earth and Planetary Sciences, 40*, 495–520. https://doi.org/10.1146/annurev-earth-040809-152540

Black, L. P., Kamo, S. L., Allen, C. M., Davis, D. W., Aleinikoff, J. N., Valley, J. W., … Foudoulis, C. (2004). Improved $^{206}Pb/^{238}U$ microprobe geochronology by the monitoring of trace-element-related matrix effect; SHRIMP, ID-TIMS, ELA-ICP-MS and oxygen isotope documentation for a series of zircon standards. *Chemical Geology, 205*, 115–140. https://doi.org/10.1016/j.chemgeo.2004.01.003

Blewett, R. S., & Black, L. P. (1998). Structural and temporal framework of the Coen Region, north Queensland: Implications for major tectonothermal events in east and north Australia. *Australian Journal of Earth Sciences, 45*, 597–609. https://doi.org/10.1080/08120099808728415

Buys, J., Spandler, C., Holm, R. J., & Richards, S. W. (2014). Remnants of ancient Australia in Vanuatu: Implications for crustal evolution in island arcs and tectonic development of the southwest Pacific. *Geology, 42*, 939–942. https://doi.org/10.1130/G36155.1

Champion, D. C., & Bultitude, R. J. (2013). Kennedy igneous association. In P. A. Jell (Ed.), *Geology of Queensland* (pp. 473–514). Brisbane: Geological Survey of Queensland.

Chiaradia, M., Merino, D., & Spikings, R. (2009). Rapid transition to long-lived deep crustal magmatic maturation and the formation of giant porphyry-related mineralization (Yanacocha, Peru). *Earth and Planetary Science Letters, 288*, 505–515. https://doi.org/10.1016/j.epsl.2009.10.012

Cloos, M., Sapiie, B., van Ufford, A. Q., Weiland, R. J., Warren, P. Q., & McMahon, T. P. (2005). *Collisional delamination in New Guinea: The geotectonics of subducting slab breakoff* (Special Paper, p. 400). Boulder: Geological Society of America.

Corfu, F., Hanchar, J. M., Hoskin, P. W. O., & Kinny, P. (2003). Atlas of zircon textures. In J. M. Hanchar & P. W. O. Hoskin (Eds.), *Reviews in mineralogy & geochemistry 53: Zircon*. Chantilly: Mineralogical Society of America.

Crowley, J. L., Schoene, B., & Bowring, S. A. (2007). U-Pb dating of zircon in the Bishop Tuff at the millennial scale. *Geology, 35*, 1123–1126. https://doi.org/10.1130/G24017A.1

Davies, H. L. (2012). The geology of New Guinea—The cordilleran margin of the Australian continent. *Episodes, 35*, 87–102.

Davies, H. L., & Jaques, A. L. (1984). Emplacement of ophiolite in Papua New Guinea. *Geological Society, London, Special Publications, 13*, 341–349. https://doi.org/10.1144/GSL.SP.1984.013.01.27

Davies, H. L., & Smith, I. E. (1971). Geology of Eastern Papua. *Geological Society of America Bulletin, 82*, 3299–3312. https://doi.org/10.1130/0016-7606(1971)82[3299:GOEP]2.0.CO;2

Dow, D. B., Smit, J. A. J., Page, R. W. (1974). *Wau–1:250,000 Geological Series. Explanatory notes to accompany Wau 1:250,000 geological map: Geological Survey of Papua New Guinea*. Explanatory Notes SB/55-14.

Drummond, B. J., Collins, C. D. N., & Gibson, G. (1979). The crustal structure of the Gulf of Papua and north-west Coral Sea. *BMR Australian Journal of Geology and Geophysics, 4*, 341–351.

Eilon, Z., Abers, G. A., Gaherty, J. B., & Jin, G. (2015). Imaging continental breakup using telesiesmic body waves: The Woodlark Rift, Papua New Guinea. *Geochemistry, Geophysics, Geosystems, 16*, 2529–2548. https://doi.org/10.1002/2015GC005835

Fergusson, C. L., Henderson, R. A., Fanning, C. M., & Withnall, I. W. (2007). Detrital zircon ages in Neoproterozoic to Ordovician siliciclastic rocks, northern Australia: Implications for the tectonic history of the East Gondwana continental margin. *Journal of the Geological Society, 164*, 215–225. https://doi.org/10.1144/0016-76492005-136

Fergusson, C. L., Henderson, R. A., & Offler, R. (2017). Late Neoproterozoic to early Mesozoic sedimentary rocks of the Tasmanides, eastern Australia: Provenance switching associated with development of the East Gondwana active margin. In R. Mazumder (Ed.), *Sediment Provenance* (pp. 325–369). Netherlands: Elsevier. https://doi.org/10.1016/B978-0-12-803386-9.00013-7

Fergusson, C. L., Henderson, R. A., Withnall, I. W., & Fanning, C. M. (2007). Structural history of the Greenvale Province, north Queensland: Early Palaeozoic extension and convergence on the Pacific margin of Gondwana. *Australian Journal of Earth Sciences, 54*, 573–595. https://doi.org/10.1080/08120090701188970

Floyd, P. A., & Winchester, J. A. (1978). Identification and discrimination of altered and metamorphosed volcanic rocks using immobile elements. *Chemical Geology, 21*, 291–306. https://doi.org/10.1016/0009-2541(78)90050-5

Gehrels, G. (2014). Detrital zircon U-Pb geochronology applied to tectonics. *Annual Review of Earth and Planetary Sciences, 42*, 127–149. https://doi.org/10.1146/annurev-earth-050212-124012

Gill, J. B. (1981). *Orogenic Andesites and plate tectonics*. Berlin: Springer-Varlag. https://doi.org/10.1007/978-3-642-68012-0

Graham, I. J., & Korsch, R. J. (1990). Age and provenance of granitoid clasts in Moeatoa Conglomerate, Kawhia Syncline, New Zealand. *Journal of the Royal Society of New Zealand, 20*, 25–39. https://doi.org/10.1080/03036758.1990.10426731

Hall, R. (2002). Cenozoic geological and plate tectonic evolution of SE Asia and the SW Pacific: Computer-based reconstructions, model and animations. *Journal of Asian Earth Sciences, 20*, 353–431. https://doi.org/10.1016/S1367-9120(01)00069-4

Heaman, L. M., Bowins, R., & Crocket, J. (1990). The chemical composition of igneous zircon suites: Implications for geochemical tracer studies. *Geochimica et Cosmochimica Acta, 54*, 1597–1607. https://doi.org/10.1016/0016-7037(90)90394-Z

Henderson, R. A. (1986). Geology of the Mt Windsor subprovince—A lower Palaeozoic volcano-sedimentary terrane in the northern Tasman orogenic zone. *Australian Journal of Earth Sciences, 33*, 343–364. https://doi.org/10.1080/08120098608729371

Hidaka, H., Shimizu, H., & Adachi, M. (2002). U-Pb geochronology and REE geochemistry of zircons from Palaeoproterozoic paragneiss clasts in the Mesozoic Kamiaso conglomerate, central Japan: Evidence for an Archean provenance. *Chemical Geology, 187*, 279–293. https://doi.org/10.1016/S0009-2541(02)00058-X

Holm, R. J., Spandler, C., & Richards, S. W. (2013). Melanesian arc far-field response to collision of the Ontong Java Plateau: Geochronology and petrogenesis of the Simuku Igneous Complex, New Britain, Papua New Guinea. *Tectonophysics, 603*, 189–212. https://doi.org/10.1016/j.tecto.2013.05.029

Holm, R. J., Spandler, C., & Richards, S. W. (2015). Continental collision, orogenesis and arc magmatism of the Miocene Maramuni arc, Papua New Guinea. *Gondwana Research, 28*, 1117–1136. https://doi.org/10.1016/j.gr.2014.09.011

Holm, R. J., Rosenbaum, G., & Richards, S. W. (2016). Post 8 Ma reconstruction of Papua New Guinea and Solomon Islands: Microplate tectonics in a convergent plate boundary setting. *Earth-Science Reviews, 156*, 66–81. https://doi.org/10.1016/j.earscirev.2016.03.005

Hoskin, P. W. O., & Schaltegger, U. (2003). The composition of zircon and igneous and metamorphic petrogenesis. In J. M. Hanchar & P. W. O. Hoskin (Eds.), *Reviews in Mineralogy & Geochemistry 53: Zircon*. Chantilly: Mineralogical Society of America.

Irvine, T. N., & Baragar, W. R. A. (1971). A guide to the chemical classification of the common volcanic rocks. *Canadian Journal of Earth Sciences, 8*, 523–548. https://doi.org/10.1139/e71-055

Jackson, S. E., Pearson, N. J., Griffin, W. L., & Belousova, E. E. (2004). The application of laser ablation-inductively coupled plasma-mass spectrometry to *in situ* U-Pb zircon geochronology. *Chemical Geology, 211*, 47–69. https://doi.org/10.1016/j.chemgeo.2004.06.017

Jakeš, P., & Smith, I. E. M. (1970). High potassium calc-alkaline rocks from Cape Nelson, eastern Papua. *Contributions to Mineralogy and Petrology, 28*, 259–271. https://doi.org/10.1007/BF00388948

Kemp, A. I. S., Hawkesworth, C. J., Collins, W. J., Gray, C. M., Blevin, P. L., & EIMF. (2009). Isotopic evidence for rapid continental growth in an extensional accretionary orogen: The Tasmanides, eastern Australia. *Earth and Planetary Science Letters, 284*, 455–466. https://doi.org/10.1016/j.epsl.2009.05.011

Kennedy, A. K., Wotzlaw, J.-F., Schaltegger, U., Crowley, J. L., & Schmitz, M. (2014). Eocene zircon reference material for microanalysis of U-Th-Pb isotopes and trace elements. *The Canadian Mineralogist, 52*, 409–421. https://doi.org/10.3749/canmin.52.3.409

Kopi, G., Findlay, R. H., & Williams, I. (2000). *Age and provenance of the Owen Stanley Metamorphic Complex*. East Papuan Composite Terrane, Papua New Guinea: Geological Survey of Papua New Guinea, Report. (unpublished).

Korsch, R. J., Adams, C. J., Black, L. P., Foster, D. A., Murray, C. G., Foudoulis, C., & Griffin, W. L. (2009). Geochronology and provenance of the Late Paleozoic accretionary wedge and Gympie Terrane, New England Orogen, eastern Australia. *Australian Journal of Earth Sciences, 56*, 655–685. https://doi.org/10.1080/08120090902825776

Lamminen, J., Andersen, T., & Nystuen, J. P. (2015). Provenance and rift basin architecture of the Neoproterozoic Hedmark Basin, South Norway inferred from U-Pb ages and Lu-Hf isotopes of conglomerate clasts and detrital zircons. *Geological Magazine, 152*, 80–105. https://doi.org/10.1017/S0016756814000144

Le Maitre, R. W. (Ed.). (2002). *Igneous rocks: A classification and glossary of terms* (2nd ed., pp. 236). Cambridge: Cambridge University Press.

Ludwig, K. R. (2009). *User's manual for isoplot 3.70: A geochronological toolkit for microsoft excel*. Berkeley: Berkeley Geochronology Center Special Publication No. 4.

Lus, W. Y., McDougall, I., & Davies, H. L. (2004). Age of the metamorphic sole of the Papuan Ultramafic Belt ophiolite, Papua New Guinea. *Tectonophysics, 392*, 85–101. https://doi.org/10.1016/j.tecto.2004.04.009

Macpherson, C. G., Dreher, S. T., & Thirlwall, M. F. (2006). Adakites without slab melting: High pressure differentiation of island arc magma, Mindanao, the Philippines. *Earth and Planetary Science Letters, 243*, 581–593. https://doi.org/10.1016/j.epsl.2005.12.034

Milsom, J., & Smith, I. E. (1975). Southeastern Papua: Generation of thick crust in a tensional environment. *Geology, 3*, 117–120. https://doi.org/10.1130/0091-7613(1975)3<117:SPGOTC>2.0.CO;2

Mortimer, N., Hauff, F., & Calvert, A. T. (2008). Continuation of the New England Orogen, Australia, beneath the Queensland Plateau and Lord Howe Rise. *Australian Journal of Earth Sciences, 55*, 195–209. https://doi.org/10.1080/08120090701689365

Næraa, T., Scherstén, A., Rosing, M. T., Kemp, A. I. S., Hoffmann, J. E., Kokfelt, T. F., & Whitehouse, M. J. (2012). Hafnium isotope evidence for a transition in the dynamics of continental growth 3.2 Gyr ago. *Nature, 485*, 627–630. https://doi.org/10.1038/nature11140

Ott, B., & Mann, P. (2015). Late Miocene to Recent formation of the Aure-Moresby fold-thrust belt and foreland basin as a consequence of Woodlark microplate rotation, Papua New Guinea. *Geochemistry, Geophysics, Geosystems, 16*, 1988–2004. https://doi.org/10.1002/2014GC005668

Paquette, J.-L., & Le Pennec, J.-L. (2012). 3.8 Ga zircons sampled by Neogene ignimbrite eruptions in Central Anatolia. *Geology, 40*, 239–242. https://doi.org/10.1130/G32472.1

Parrish, R. R. (1990). U-Pb dating of monazite and its application to geological problems. *Canadian Journal of Earth Sciences, 27*, 1431–1450. https://doi.org/10.1139/e90-152

Peccerillo, A., & Taylor, S. R. (1976). Geochemistry of Eocene calc-alkaline volcanic rocks from the Kastamonu area, Northern Turkey. *Contributions to Mineralology and Petrology, 58*, 68–81.

Pell, S. D., Williams, I. S., & Chivas, A. R. (1997). The use of protolith zircon-age fingerprints in determining the protosource areas for some Australian dune sands. *Sedimentary Geology, 109*, 233–260. https://doi.org/10.1016/S0037-0738(96)00061-9

Pieters, P. E. (1978). Port Moresby-Kalo-Aroa, Papua New Guinea - 1:250 000 Geological Map Series (p. 55). BMR Australia Explanatory Notes.

Pirard, C., & Spandler, C. (2017). The zircon record of high-pressure metasedimentary rocks of New Caledonia: Implications for regional tectonics of the south-west Pacific. *Gondwana Research, 46*, 79–94. https://doi.org/10.1016/j.gr.2017.03.001

Samuel, M. D., Be'eri-Shlevin, Y., Azer, M. K., Whitehouse, M. J., & Moussa, H. E. (2011). Provenance of conglomerate clasts from the volcano-sedimentary sequence at Wadi Rutig in southern Sinai, Egypt as revealed by SIMS U-Pb dating of zircon. *Gondwana Research, 20*, 450–464. https://doi.org/10.1016/j.gr.2010.11.021

Schärer, U. (1984). The effect of initial ^{230}Th disequilibrium on young U-Pb ages: The Makalu case, Himalaya. *Earth and Planetary Science Letters, 67*, 191–204. https://doi.org/10.1016/0012-821X(84)90114-6

Schellart, W. P., Lister, G. S., & Toy, V. G. (2006). A late cretaceous and Cenozoic reconstruction of the Southwest Pacific region: Tectonics controlled by subduction and slab rollback processes. *Earth-Science Reviews, 76*, 191–233. https://doi.org/10.1016/j.earscirev.2006.01.002

Schott, R. C., & Johnson, C. M. (2001). Garnet-bearing trondhjemite and other conglomerate clasts from the Gualala basin, California: Sedimentary record of the missing western portion of the Salinian magmatic arc? *Geological Society of America Bulletin, 113*, 870–880. https://doi.org/10.1130/0016-7606(2001)113<0870:GBTAOC>2.0.CO;2

Shaanan, U., Rosenbaum, G., Hoy, D., & Mortimer, N. (2018). Late Paleozoic geology of the Queensland Plateau (offshore northeastern Australia). *Australian Journal of Earth Sciences*. doi: https://doi.org/10.1080/08120099.2018.1426041

Shearman, P., & Bryan, J. (2011). A bioregional analysis of the distribution of rainforest cover, deforestation and degradation in Papua New Guinea. *Austral Ecology, 36*, 9–24. https://doi.org/10.1111/aec.2011.36.issue-1

Shearman, P. L., Ash, J., Mackey, B., Bryan, J. E., & Lokes, B. (2009). Forest conversion and degradation in Papua New Guinea 1972–2002. *Biotropica, 41*, 379–390. https://doi.org/10.1111/btp.2009.41.issue-3

Smith, I. E. (1972). High-potassium intrusives from southeastern Papua. *Contributions to Mineralogy and Petrology, 34*, 167–176. https://doi.org/10.1007/BF00373771

Smith, I. E. M. (1976). *Volcanic rocks from southeastern Papua: The Evolution of volcanism at a plate boundary* (Unpublished PhD Thesis, p. 298). Canberra: Australian National University.

Smith, I. E. (1982). Volcanic evolution in eastern Papua. *Tectonophysics, 87*, 315–333. https://doi.org/10.1016/0040-1951(82)90231-1

Smith, I. E. M. (2013a). The chemical characterization and tectonic significance of ophiolite terrains in southeastern Papua New Guinea. *Tectonics, 32*, 1–12.

Smith, I. E. M. (2013b). High-magnesium andesites: The example of the Papuan Volcanic Arc. In A. Gómez-Tuena, S. M. Straub, & G. F. Zellmer (Eds.), *Orogenic andesites and crustal growth* (p. 385). London: Geological Society, Special Publications.

Smith, I. E., & Davies, H. L. (1976). Geology of the southeast Papuan mainland. *BMR Journal of Australian Geology and Geophysics, 165*, 86p.

Smith, I. E., & Milsom, J. S. (1984). Late Cenozoic volcanism and extension in Eastern Papua. *Geological Society, London, Special Publications, 16*, 163–171. https://doi.org/10.1144/GSL.SP.1984.016.01.12

Stacey, J. S., & Kramers, J. D. (1975). Approximation of terrestrial lead isotope evolution by a two-stage model. *Earth and Planetary Science Letters, 26*, 207–221. https://doi.org/10.1016/0012-821X(75)90088-6

Sun, S., & McDonough, W. F. (1989). Chemical and isotopic systematics of oceanic basalts: Implications for mantle composition and processes. *Geological Society, London, Special Publications, 42*, 313–345. https://doi.org/10.1144/GSL.SP.1989.042.01.19

Tapster, S., Roberts, N. M. W., Petterson, M. G., Saunders, A. D., & Naden, J. (2014). From continent to intra-oceanic arc: Zircon xenocrysts record the crustal evolution of the Solomon island arc. *Geology, 42*, 1087–1090. https://doi.org/10.1130/G36033.1

Taylor, B., Goodliffe, A., Martinez, F., & Hey, R. (1995). Continental rifting and initial sea-floor spreading in the Woodlark basin. *Nature, 374*, 534–537. https://doi.org/10.1038/374534a0

Taylor, B., Goodliffe, A. M., & Martinez, F. (1999). How continents break up: Insights from Papua New Guinea. *Journal of Geophysical Research: Solid Earth, 104*, 7497–7512. https://doi.org/10.1029/1998JB900115

Tera, F., & Wasserburg, G. J. (1972). U-Th-Pb systematics in three Apollo 14 basalts and the problem of initial Pb in

lunar rocks. *Earth and Planetary Science Letters, 14*, 281–304. https://doi.org/10.1016/0012-821X(72)90128-8

Van Achterbergh, E., Ryan, C. G., Jackson, S. E., Griffin, W. L. (2001). Appendix. In P. J. Sylvester (Ed.), *Laser Ablation-ICP-Mass Spectrometry in the Earth Sciences: Principle and Applications* (Vol. 29, p. 239). Ottawa, ON: Mineralog. Assoc. Can. (MAC) Short Course Series.

Van Wyck, N., & Williams, I. S. (2002). Age and provenance of basement metasediments from the Kubor and Bena Bena Blocks, central Highlands, Papua New Guinea: Constraints on the tectonic evolution of the northern Australian cratonic margin. *Australian Journal of Earth Sciences, 49*, 565–577. https://doi.org/10.1046/j.1440-0952.2002.00938.x

Wallace, L. M., Ellis, S., Little, T., Tregoning, P., Palmer, N., Rosa, R., ... Kwazi, J. (2014). Continental breakup and UHP rock exhumation in action: GPS results from the Woodlark Rift, Papua New Guinea. *Geochemistry, Geophysics, Geosystems, 15*, 4267–4290. https://doi.org/10.1002/2014GC005458

Wandres, A. M., Bradshaw, J. D., Weaver, S., Maas, R., Ireland, T., & Eby, N. (2004). Provenance analysis using conglomerate clast lithologies: A case study from the Pahau terrane of New Zealand. *Sedimentary Geology, 167*, 57–89. https://doi.org/10.1016/j.sedgeo.2004.02.002

Webb, L. E., Baldwin, S. L., & Fitzgerald, P. G. (2014). The early-middle miocene subduction complex of the louisiade archipelago, southern margin of the woodlark rift. *Geochemistry, Geophysics, Geosystems, 15*, 4024–4046. https://doi.org/10.1002/2014GC005500

Whattam, S. A., Malpas, J., Ali, J. R., & Smith, I. E. M. (2008). New SW Pacific tectonic model: Cyclical intraoceanic magmatic arc construction and near-coeval emplacement along the Australia-Pacific margin in the Cenozoic. *Geochemistry, Geophysics, Geosystems, 9*, Q03021.

Worthing, M. A., & Crawford, A. J. (1996). The igneous geochemistry and tectonic setting of metabasites from the Emo Metamorphics, Papua New Guinea; a record of the evolution and destruction of a backarc basin. *Mineralogy and Petrology, 58*, 79–100. https://doi.org/10.1007/BF01165765

Cogent Geoscience (ISSN: 2331-2041) is published by Cogent OA, part of Taylor & Francis Group.

Publishing with Cogent OA ensures:

- Immediate, universal access to your article on publication
- High visibility and discoverability via the Cogent OA website as well as Taylor & Francis Online
- Download and citation statistics for your article
- Rapid online publication
- Input from, and dialog with, expert editors and editorial boards
- Retention of full copyright of your article
- Guaranteed legacy preservation of your article
- Discounts and waivers for authors in developing regions

Submit your manuscript to a Cogent OA journal at www.CogentOA.com